

Monitoring the temporal-spatial changes of vegetation cover and drivers in Tian Shan ecoregions, China

Seyed Omid Reza Shobairi^{1,2}, *Sun Lingxiao*^{1,2} ✉, *Zhang Haiyan*^{1,2}, *Li Chunlan*^{1,2}, *He Jing*^{1,2}, *Behnam Asghari Beirami*³

¹ Chinese Academy of Sciences, Xinjiang Institute of Ecology and Geography, Urumuqi, 830011, China, sunlx@ms.xjb.ac.cn

² University of Chinese Academy of Sciences, Beijing, 100049, China

³ K.N. Toosi University of Technology, Department of Photogrammetry and Remote Sensing, Tehran, Iran

ABSTRACT

This study analyzed satellite data from 2000 to 2022 in the Tian Shan ecoregions of northwestern China to investigate relationships between climate, environment, soil conditions, and human activities on constantly changing vegetation fluctuations. The NDVI index outperformed EVI over the period, with peak values of 0.56 and 0.33, respectively. NDVI trends indicated a higher slope of 5.15 compared to 4.91 for EVI. Analysis showed that vegetation area had expanded over time, with the lowest coverage between 2000 and 2005, but then, it spread due to varying degree of human activities' impacts from 0 to 63. Tests revealed significant negative correlations between soil moisture and EVI/NDVI indexes attributed to natural water phenomena causing vegetation stress. Positive correlations were found between EVI/NDVI with actual evapotranspiration and snow, while negative with wind speed and radiation. The study also found a positive correlation between NDVI and measures of human activity, indicating restoration efforts, project implementations, and soil management preventing erosion expanded vegetation. Overall, the study concluded that human activities had a greater influence than climate through water and soil preservation, resulting in more vegetation expansion over time. Indigenous resource concepts also significantly contributed to long-term preservation efforts evidently maintaining and strengthening vegetation in the ecoregions. These findings highlight the efficacy and resilience of human activity in overcoming climatic and environmental challenges. While human factors can potentially harm the environment and renewable resources, long-term planning and preservation efforts, as evident in the Tian Shan ecoregions, have successfully preserved and strengthened the vegetation.

KEY WORDS

NDVI, EVI, ecoregion, climate change, drivers, GEE

INTRODUCTION

Vegetation, defined as the proportion of land surface covered by plants, is influenced by climate change, the natural environment, and human activity (Jing et al. 2011). It is a crucial part of terrestrial ecosystems, playing a vital role in regulating the Earth's carbon balance and climate system (Liu et al. 2018). The diversity of vegetation is significantly affected by these factors (Nemani et al. 2003). Climate factors influence long-term vegetation growth patterns and the distribution of onshore vegetation, affecting regional ecosystem services. Human activities, on the other hand, have altered vegetation's geographical range and growth quality in shorter timeframes, significantly impacting regional ecosystem services and functions (Hu et al. 2019; Rull et al. 2011). Identifying the relationship and significance of each parameter in relation to changes in land cover is essential (Liu et al. 2018; Shen et al. 2016). Modern remote sensing techniques are valuable for accurately monitoring global vegetation dynamics, enhancing our understanding of biosphere processes and their interactions with Earth's climate.

Climate factors are crucial for long-term vegetation growth trends, influencing onshore vegetation distribution and regional ecosystem services, while human activities have significantly altered vegetation's geographical range and quality in shorter timeframes, impacting regional ecosystem services (Hu et al. 2019; Rull et al. 2011). Identifying the relationships and significance of these parameters concerning land cover changes is essential (Liu et al. 2018; Shen et al. 2016). Modern remote sensing techniques are valuable tools for accurately monitoring global vegetation dynamics, enhancing the understanding of biosphere processes and their climate interactions.

Various spectral indicators from satellite data, such as the NDVI, have been used to evaluate spatial patterns and trends of human activity and climate change impacts on vegetation and biomass, showing a close connection to vegetation activity (Tucker 1979). Researchers have conducted comprehensive studies on this relationship (Eastman et al. 2013; Sharma et al. 2022; Zhang et al. 2013). Climatic variables like air temperature and precipitation are significant for vegetation indicators (Gao et al. 2022; Shang et al. 2022; Sun et al. 2021; Gao et al. 2021), regulating vegetation growth (Wang et al. 2016; Braswell et al. 1997; Guo et al. 2021). For instance, Wang et al. (2016) used NDVI data to study vegetation phe-

nology in the Northern Hemisphere from 1982 to 2012, showing how vegetation in different ecological zones responds to climate change. Climate change affects vegetation growth periods, composition, and morphology (Liu and Lei 2015; Sun et al. 2015; Deng and Chen 2017), with precipitation and temperature being primary drivers (Sun et al. 2021; Gao et al. 2022; Gao et al. 2021).

Shang et al. (2022) identified these as key factors influencing NDVI changes in northwest China. Zhou et al. (2019) found a negative correlation between elevation and vegetation. Deng et al. (2020) noted that karst areas have high soil moisture, which decreases rapidly compared to non-karst areas, impacting vegetation growth. Human activities also impact vegetation through deforestation, pollution, and habitat destruction, but can also preserve biodiversity through restoration and sustainable practices (Shi et al. 2021; Fyfe 2023; Meredith and Jens 2018). Thus, human impacts have both constructive and destructive implications.

This research aims to analyze vegetation changes in the Tian Shan Ecoregions over the last 23 years using remote sensing data. It investigates the connections between vegetation dynamics and climate, soil characteristics, surface features, and human activities, providing insights into terrestrial ecosystem responses to climate fluctuations. ArcGIS and coding techniques are utilized to predict the impacts of various biotic and abiotic factors on vegetation indexes.

RESEARCH SIGNIFICANT

This study develops a method of monitoring vegetation dynamics at the ecological scale of the Tian Shan ecoregions and also helps to predict the future of fragile ecosystems of rare plant and animal species in northwest China and Central Asia, which lies behind these changes, climate change scenarios and human-induced activities.

MATERIAL AND METHODS

Xinjiang province, located in northwest China (Jiapaer et al. 2015), covers 1.66 million km², about one-sixth of China's total area (Yu et al. 2020). It's a fragile ecological zone with 51.4% mountainous and 48.6% plains (Luo et al. 2019; Jiapaer et al. 2015). The region fea-

tures diverse landforms, including the Altai, Kunlun, A-erh-chin, and Tian Shan mountains, which enclose the Junggar and Tarim Basins (Zhao et al. 2022; Luo et al. 2019). Forests and grasslands make up 31.29% of the area, with grasslands predominating (Zhuang et al. 2020). The northern region receives more rainfall (100–500 mm) and has cooler temperatures (4–8°C), while the south is drier (20–100 mm) and warmer (10–13°C) (Cao and Gao 2022).

Table 1. 17 ecoregions of Xinjiang province. The area of all three Tian Shan ecoregions is well calculated.

Ecoregions	Area, km ²	Percent
Alashan Plateau semi-desert	67	16.498
Altai alpine meadow and tundra	90,434	2.212
Altai montane forest and forest steppe	142,875	3.495
Altai steppe and semi-desert	83,192	2.035
Central Tibetan Plateau alpine steppe	629,190	15.393
Emin Valley steppe	65,135	1.594
Junggar Basin semi-desert	304,938	7.460
Karakoram-West Tibetan Plateau alpine steppe	143,265	3.505
North Tibetan Plateau-Kunlun Mountains alpine desert	374,494	9.162
Pamir alpine desert and tundra	118,072	2.889
Qaidam Basin semi-desert	192,147	4.701
Rock and Ice	34,830	0.852
Taklimakan desert	742,657	18.169
Tarim Basin deciduous forests and steppe	54,533	1.334
Tian Shan foothill arid steppe	129,231	3.162
Tian Shan montane conifer forests	27,568	0.674
Tian Shan montane steppe and meadows	280,611	6.865

Ecoregions, distinct areas with consistent ecosystems, are crucial for environmental assessment (Lovland and Merchant 2004). The Ecoregion data for Xinjiang come from <https://ecoregions.appspot.com>; <https://www.oneearth.org/>, revealing 17 ecoregions and 5 biomes, with the Taklimakan desert and Tian Shan montane conifer forests being the largest and smallest, respectively. The current research focuses on the Tian Shan ecoregions (Fig. 1), divided into three: Tian Shan foothill arid steppe, Tian Shan montane conifer for-

ests, and Tian Shan montane steppe and meadows. Our analysis primarily revolves around the examination of primary data related to these specific ecoregions.

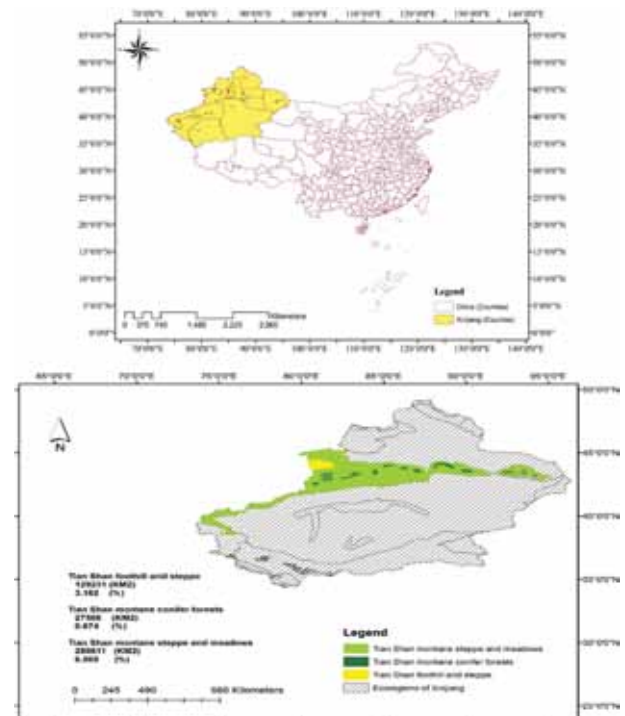

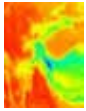



Figure 1. Geographical location of the Tian Shan ecoregions by calculating the area of each three ecoregions in square kilometers and a percentage composed of the whole Xinjiang province

The Tian Shan foothill arid steppe (WWF ID: PA0818) spans the northern and western Tian Shan, featuring semi-arid and humid climates with diverse vegetation and wildlife (Kottek et al. 2006; <https://ecoregions.appspot.com>; <https://www.worldwildlife.org/>). The Tian Shan montane conifer forests (WWF ID: PA0521) cover north-facing slopes between 1,500 and 2,700 meters, dominated by Asian spruce and mixed with other trees at different elevations (<https://ecoregions.appspot.com>; <https://www.worldwildlife.org/>). The Tian Shan montane steppe and meadows (WWF ID: PA1019) stretch along the Tian Shan ridge, featuring grasslands at various altitudes and acting as a barrier between the Tarim Basin, Taklimakan Desert, Junggar Basin, and Kazakh Shield. This ecoregion supports diverse species due to its large size and range of altitudes (Kottek et al. 2006; <https://www.worldwildlife.org/>).

Table 2. Main sources with the satellite product specifications

Insignia	Product	Parameter	Temporal coverage		Description	Website details
	MYD13A1.061	NDVI	16 Daily		Normalized Difference Vegetation Index	https://developers.google.com/earth-engine/datasets/catalog/MODIS_061_MYD13A1
	ERA5-Land	Temperature	Daily		ECMWF Climate Reanalysis	https://developers.google.com/earth-engine/datasets/catalog/ECMWF_ERA5_LAND_DAILY_AGGR#bands
Evaporation						
Runoff						
	CHIRPS	Precipitation	Daily		Hazards Group InfraRed	https://developers.google.com/earth-engine/datasets/catalog/UCSB-CHG_CHIRPS_DAILY
Product	Band	Image collection	Value		Units	Time and dataset availability
			Min	Max		
MYD13A1.061	NDVI	MODIS/061/MYD13A1	-2000	10000	--	2002-07-04T00:00:00Z–2023-06-18T00:00:00
ERA5-Land	temperature_2m	ECMWF/ERA5_LAND/D	--	--	K	1950-01-02T00:00:00Z–2023-07-26T00:00:00
	total_evaporation_sum	AI	--	--	m of water equivalent	
	runoff_sum	LY_AGGR	--	--	m	
CHIRPS	Precipitation	CSB-CHG/CHIRPS/DAILY	0*	1444.34*	mm/d	1981-01-01T00:00:00Z–2023-06-30T00:00:00
Satellite/model	Product name	Data name	Unit	Spatial resolution	Temporal resolution	Time extent
Modis/Terra	MOD11A1.061 Terra Land Surface Temperature and Emissivity Daily Global 1 km	LST_Day_1km	Kevin	1000 meters	Daily	2000-02-24
Modis/Terra	Vegetation Indices	NDVI EVI	-	500 meters	Daily	2000-02-18
FLDAS	FEWS NET	Soil Moisture	m ³ m-3	10 km	Monthly	1/1/1982
		Shortwave Radiation Flux	w m-2	--	--	
TERRA Climate	University of IDAHO	Palmer Drought Index	nan	--	--	1/1/1958
		Wind Speed	m/s	4 km	Monthly	
Satellite/model	Product name	Date name	Unit	Spatial resolution	Temporal coverage	Time extent
MODIS	MODIS Land Cover Type (LC_Type2 Class Table)	MCD12Q1.061	-	500 m	Yearly	2001-01-01T00:00:00Z–2022-01-01T00:00:00 ee.ImageCollection("MODIS/061/MCD12Q1")

The calculated satellite data are based on modeling this study. With the help of the Google Earth Engine (GEE) platform and its raster file catalogs, calculations went forward. MODIS/061/MYD13A1-NDVI 16 daily (2000 to 2023) with a spatial resolution of 250-m Global scale and drivers datasets, such as air temperature at 2 m, total precipitation, LST, actual evaporation, runoff, soil moisture, wind speed, palmer drought severity index (PDSI), downward surface shortwave radiation (DSR), and snow water equivalent, were extracted from ERA5-Land, CHIRPS, for a 23-year period. Data are available through <https://code.earthengine.google.com>. MODIS LULC data (MCD12Q1.061) were also excavated to track human activities and calculate the areas of vegetation and land. The main sources and characteristics of the collected data are listed in Table 2.

Raster calculations of plant indicators and climatic and environmental parameters

Average value of the vegetation indices and their changes attributed to climate and environment parameters were examined based on annual, pixel-wise trends in NDVI, EVI, LST daytime, total precipitation, air temperature at 2 m, actual evapotranspiration, soil moisture at 10 cm, wind speed, snow water equivalent, and DSR time series.

To the tribute that first the monthly average, then the annual average, and finally the average for all the years of the period in question from 2000 to 2022 were carefully analyzed and visualized. NDVI, EVI, and LST equations are in the following order (Cheng and Liang 2017):

$$NDVI = \frac{NIR - RED}{NIR + RED} \quad (1)$$

$$EVI = 2.5 \times \frac{(NIR - RED)}{(NIR + C_1 \times RED - C_2 \times BLUE + L)} \quad (2)$$

where:

- Blue, RED, NIR – spectral bands,
- L – corrects for soil back ground,
- C1, C2 – coefficients which are related to aerosol scattering in the atmosphere.

LST is also calculated according to the following equation (Ehsanul et al. 2021):

$$T_s = \frac{BT}{\left\{1 + \left[\frac{\lambda BT}{\rho}\right], \ln \varepsilon\right\}} - 273.15 \quad (3)$$

Total precipitation represents the combined amount of rain and snow that descends onto the Earth's surface. Monthly precipitation is calculated by adding up the daily precipitation values for each month. To determine the monthly average, the total precipitation amounts for all months are summed and divided by the number of months considered within the chosen period of 22 years. The yearly total is obtained by summing the averages of individual months.

2m Temperature refers to the air temperature measured at a height of 2 meters above the Earth's surface. The 2m Temperature Anomaly indicates the deviation of the forecasted temperature for the current day from the long-term average temperature for the same day of the year. This parameter is measured in Kelvin (K). To convert Kelvin to Celsius, the following conversion relationship is utilized:

$$C = K - 273.15 \quad (4)$$

While the size of the degree is the same in Kelvin and Celsius, the two scales are not equal at any point: A Celsius temperature is always higher than a Kelvin temperature.

Actual Evapotranspiration (*ET_a*) is the quantity of water that is removed from a surface due to the processes of evaporation and transpiration and is measured in millimeters (mm). Our remote sensing data have been gradually used to estimate actual evapotranspiration.

$$ET = kc \cdot ET_0 \quad (5)$$

where:

- ET_a* – actual evapotranspiration,
- K_c* – crop coefficient,
- ET₀* – reference evapotranspiration.

Surface soil moisture refers to the water content present in the top 10 cm of soil. A reading of 0 indicates that the soil moisture has reached the wilting point, indicating extreme dryness. Conversely, a reading of 1 signifies that the soil moisture has reached saturation, indicating a state of being highly saturated with water.

It was taken advantage of strong experimental variables such as runoff, snow water equivalent, and wind speed at 10 m, palmer drought, and at the end downward shortwave radiation (DSR) designates solar radiation

with a wavelength from 300 to 4000 nm received at the Earth's surface. It is the driving force of many global ecological, hydrological, biophysical, and biochemical processes and is a key variable in modeling weather and climate systems.

A time series model is a collection of data points arranged chronologically, with time serving as the independent variable. These models are employed to examine and predict future trends. When dealing with time series data, we analyze the patterns and variations over time, allowing us to gain insights into the concept of most time series and observe yearly fluctuations in our research.

The scatter plot ($y = mx + b$) was also generalized to analyze the correlation of two vegetation variables NDVI and EVI. We already checked the normality of the distribution of data related to plant indicators before the Shapiro–Wilk test.

Relationships between NDVI and EVI were displayed as dependent variables, with other climatic and environmental parameters and human drivers using 3D scatter plots. Indeed, 3D scatter plots are utilized to visually represent data points across three axes, aiming to illustrate the correlation between three variables. Each entry in the dataset is depicted as a marker, positioned based on its corresponding values in the columns assigned to the X, Y, and Z axes.

In order to evaluate the long-term changes in plant and climatic and environmental parameters above, in addition to comparing their mean values, we used linear regression models. In fact, the use of the slope model is a very valuable way to investigate the annual and total period anomalies of the named parameters. Hence, the linear regression slope (anomaly) was computed as follows:

$$\text{Slope} = \frac{n \sum_{i=1}^n \times NDVI_i - \sum_{i=1}^n i \times \sum_{i=1}^n NDVI_i}{n \sum_{i=1}^n i^2 - (\sum_{i=1}^n i)^2} \quad (6)$$

where:

slope – the trend of vegetation dynamics or climate and environmental variables,

n – the number of years in the study period,

i – the year and $NDVI_i$ in the i th year.

The positive slope counts increasing trends, while negative slope values display declining (decreasing) trends (Piao et al. 2011).

Correlation coefficient formula is given and explained here for all the variables:

$$r = \frac{n(\sum xy) - (\sum x)(\sum y)}{\sqrt{[n \sum x^2 - (\sum x)^2][n \sum y^2 - (\sum y)^2]}} \quad (7)$$

where:

r – defines the correlation coefficient,

y – assumed as responsive variables of NDVI and EVI,

x – considers independent experimental variables (climate, environment, and human drivers) of this research.

To assess the relationships between the mentioned variables (Mihretab et al. 2020), the Pearson correlation coefficient (r) and its associated P-value were employed. Specifically, the correlation coefficient (r) was used to gauge the strength of the connections between NDVI, EVI, and climate parameters in an environmental context. A significance level of 95% was chosen to determine the statistical significance of the correlations. The correlation coefficient (r) indicates the magnitude of the linear relationship, while the P-value represents the corresponding probability level. A positive correlation and a p-value below 0.05 indicate a statistically significant relationship between the two variables.

Undoubtedly, the correlation matrix is capable of displaying the correlation coefficient between the aforementioned variables. This matrix reveals the correlation values, which quantify the extent of the linear relationship between each pair of variables. These correlation values can range from -1 to $+1$. When the two variables tend to increase and decrease together, the correlation value is positive.

Next, as the scenario was determined which parameter had the most impact and how the variables interacted, the area values and percentage of anomalies and changes of the most important NDVI vegetation index were calculated, modeled, and visualized for the first period (2000) and the end of the period in question (2022), and we carefully extracted all the fluctuations of this index, which recounts the process of resuscitation, stillness, and degradation of vegetation with advanced coding. Benefiting from the data of MODIS LULC was also applied to track human activities and calculate the areas of various types of vegetation, forest classification, shrubs, pastures, agricultural lands, and residential areas in 2001 and 2021.

Raster calculation of harmonized global Night Time Light data and modeling human drivers

In the research study, a global Night Time Light (NTL) dataset was created by merging and standardizing NTL observations from the DMSP and simulated DMSP-like NTL observations from the VIIRS data (<https://gee-community-catalog.org/>). The dataset, covering a specific area of interest includes DMSP NTL time-series data from 2000 to 2020, revealing consistent temporal patterns valuable for studying human activities like electricity consumption, land-use changes, urban expansion, and industrialization dynamics. The dataset comprises temporally calibrated DMSP-OLS NTL data from 1992 to 2013 and converted NTL data from VIIRS spanning 2014 to 2020, with a spatial resolution of approximately 30 arc-seconds.

The provided code demonstrates how to access and utilize the dataset: <https://code.earthengine.google.com/?scriptPath=users/sat-io/awesome-gee-catalog-examples/global-utilities-assets-amenities/HARMONIZED-GLOBAL-NTL>

Additionally, the study conducted an analysis within the Tian Shan Ecoregion from 2000 to 2020, calculating the Compounded Night Light Index (CNLI) that incorporates parameters reflecting night light brightness and the extent of lit urban areas, offering insights into urban population dynamics, economic indicators, and urban growth simultaneously (Wei et al. 2014). To compute the CNLI for our specific study area, we utilized the following formula:

$$\text{CNLI Index} = I \times S \quad (8)$$

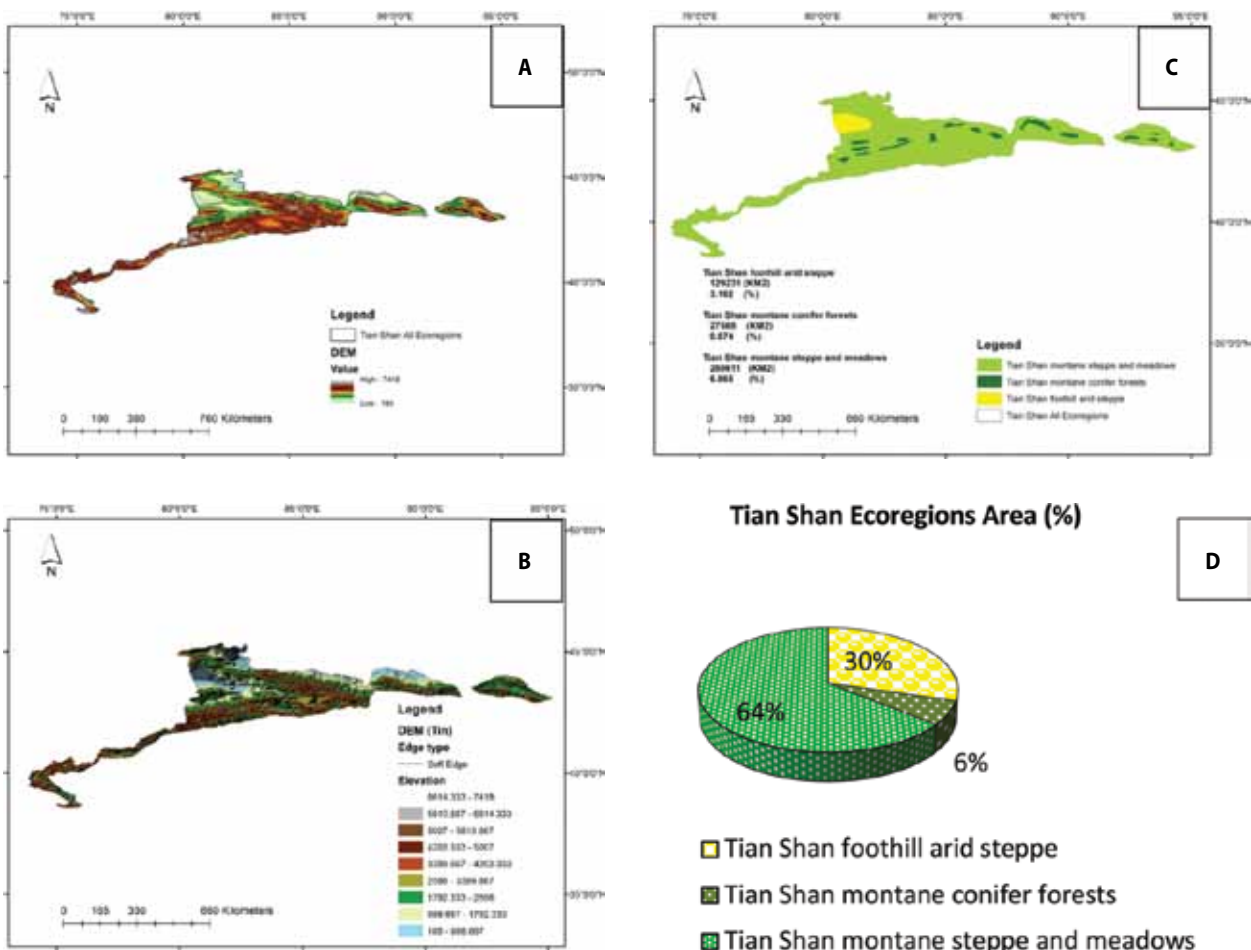


Figure 2. Geographical topography (A), elevation (B), situation (C), and area (D) of Tian Shan ecoregions during the statistical period of 2000–2022

where:

I – the average night light brightness of all lit pixels in a region.

It illustrates as follows:

$$I = \frac{1}{N_L \times DN_M} \times \sum_{i \equiv P}^{DN_M} (DN_i \times n_i) \quad (9)$$

In the formula provided, we have several variables and parameters. The variable DN_i represents the DN value associated with the i th gray level. The variable n_i represents the count of illuminated pixels corresponding to that specific gray level. The parameter P denotes the optimal threshold used to identify the illuminated urban areas within the DMSPI images. Additionally, DN_M represents the maximum DN value observed, while N_L represents the count of illuminated pixels with DN values ranging between P and DN_M . Finally, the parameter S represents the proportion of illuminated urban areas relative to the total area of a given region. The mathematical representation of S can be expressed as follows:

$$S = \frac{Area_N}{Area} \quad (10)$$

In the context provided, we have two variables: $Area_N$ represents the area occupied by illuminated urban areas within a specific region and $Area$ represents the total area of that region.

RESULTS AND DISCUSSION

In this study, we analyzed the interactions between plant indicators, climatic and environmental factors, and human drivers over 23 years in the Tian Shan ecoregions. These regions, ranging from 185 to 7418 meters above sea level, are categorized into mountain steppe/pastures, mountain coniferous forests, and dry mountain foothills. The largest area is the mountain steppes/pastures (64%; 280,311 km²), while the smallest are the mountain coniferous forests (6%; 27,568 km²) (Fig. 2).

Response variable; vegetation index

NDVI and EVI

The vegetation condition in the Tian Shan ecoregions from 2000 to 2022 was assessed using NDVI and EVI indicators. NDVI covered a wider area and exhibited a better trend than EVI, with peak values of 0.56 and

0.33, respectively, and a higher slope trend of 5.15% (Fig. 3). Regions with lower altitudes, particularly in the west, northwest, and central areas, showed higher and better vegetation trends compared to southern regions, highlighting the impact of altitude on vegetation (Fig. 4). The study indicates that lower altitudes correlate with higher and stronger vegetation indicators (NDVI and EVI) (Figure 3).

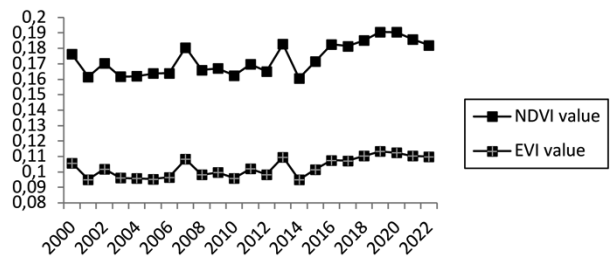


Figure 3. Trend of vegetation indices of Tian Shan ecoregions during the statistical period 2000–2022

Experimental independent variable: climate and environment parameters

Temporal and spatial patterns of LST day time (kelvin), total precipitation (mm), air temperature at 2 m (kelvin), actual evapotranspiration (mm), soil moisture at 10 cm (mm), downward shortwave radiation (DSR), snow water equivalent (SWE), and wind speed

The Tian Shan ecoregion is highly influenced by external drivers like climate parameters owing to its unique geographic location and topography. This study delves into analyzing the climate parameters within the Tian Shan ecological zone from 2000 to 2022 (based on Fig. 5–12). The findings indicate significant variations in precipitation levels over the 23-year period, with 2016 recording the highest precipitation exceeding 35 cm. On average, the region receives more than 154 mm of rainfall, with distinct patterns observed across different parts, particularly in the western, central, northeastern, and southwestern regions (Fig. 5A). The discrepancies in precipitation levels are largely attributed to the elevation differences in these areas (Fig. 5B).

The survey of the Tian Shan indigenous region's average snow-equivalent water (SWE) reveals that the 23-year average SWE ranges from 0.008 to 10061.1 mm (Fig. 6A). The anomalous slope value falls between 0.022 and -0.085 (Fig. 6B). Over the considered period, this phenomenon has shown an incremental trend,

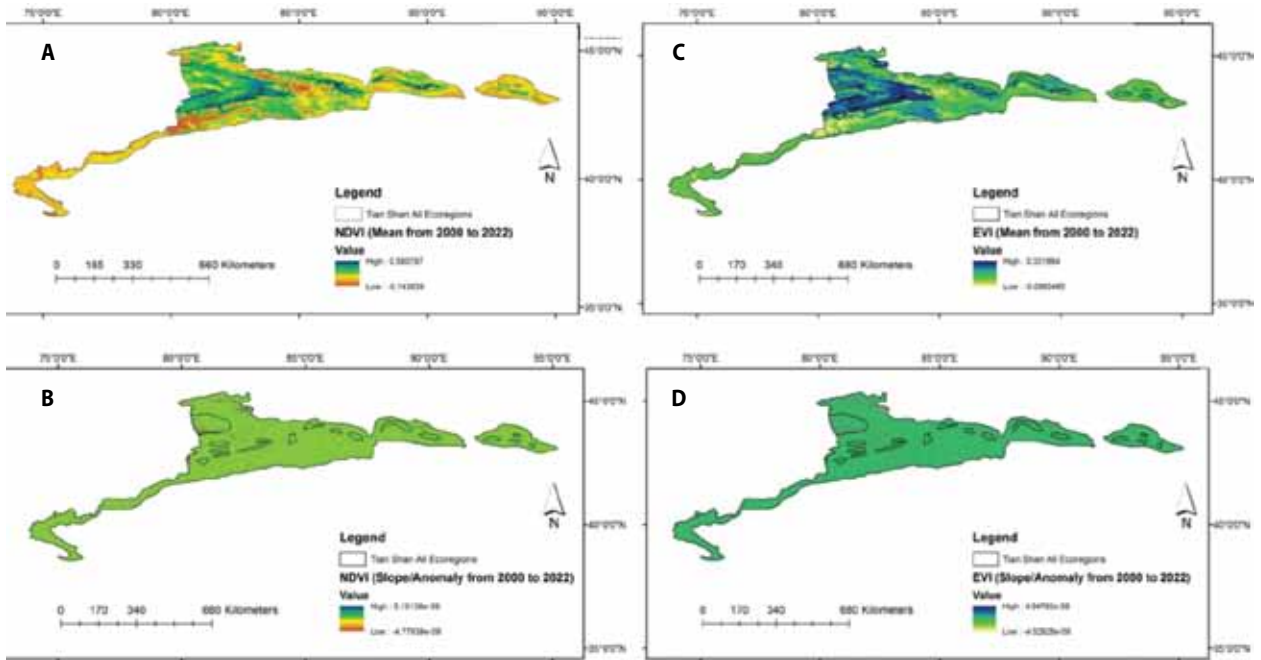


Figure 4. Temporal trend of mean NDVI (A), NDVI slop and anomaly (B), mean EVI (C), and EVI slop and anomaly (D) in Tian Shan ecoregions during the period of 2000–2022

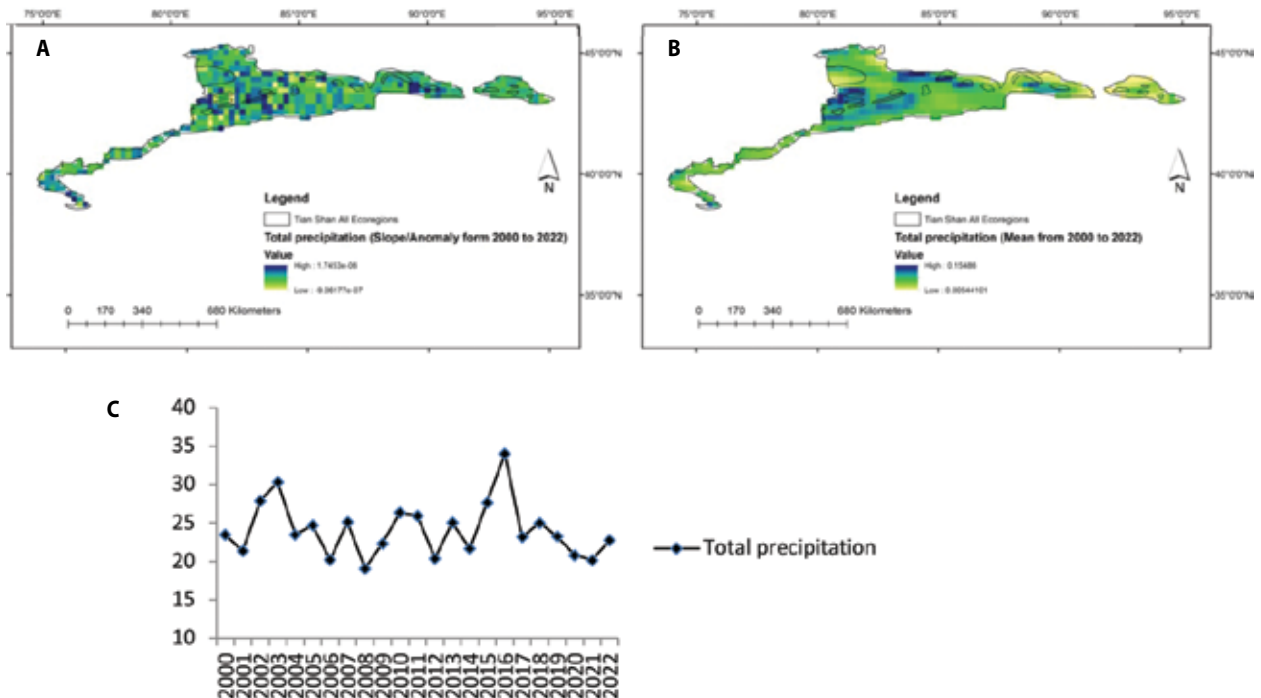


Figure 5. Changes in the total precipitation slop/anomaly(A), changes in the total precipitation mean (B), and changes in the average precipitation of the Tian Shan ecological zone during the statistical period 2000–2022 (column numbers are in centimeters) (C)

with the minimum value recorded in 2008 and a noticeable increase from 2011 onward (Fig. 6C). Snow plays a crucial role in the cold regions' ecosystem, connecting wildlife, vegetation, and soil moisture. SWE quantifies the water stored as snow on the Earth's surface and holds significant importance for water, energy, and geochemical cycles. This relationship between SWE and vegetation will be further explored in the Tian Shan ecoregion.

Soil moisture plays a significant role in vegetation growth across different regions. In the Tian Shan ecoregions, the average soil moisture ranges from 1 to 0.157 (Fig. 7A), with the highest levels observed in the western and northern areas. The anomaly value of soil moisture slope varies from 3.2 to -3.3 in this region (Fig. 7B). A soil moisture value of 0 indicates extreme dryness (wilting point), while a value of 1 represents high saturation with water. Optimal conditions for plant growth occur at a soil moisture value of 0.54, while values below 0.2 and above 0.8 indicate drought and excessive moisture stress, respectively. Further analysis will reveal a negative relationship between soil moisture and vegetation indices such as NDVI and EVI. High moisture content (equal to or greater than 0.8) results from snow melting, surface currents, and lakes exposes vegetation to additional moisture stress, leading to vegetation decline. Additionally, high soil moisture in cold seasons can cause soil texture freezing, resulting in problems for the plant root system and vegetation loss. In the southern regions, the slope value for soil moisture reaches its lowest point. The study of average soil moisture changes indicates a decreasing trend from 2015 onward, significantly impacting vegetation growth in the Tian Shan ecoregions (Fig. 7C).

Land surface temperature (LST) is a critical climate parameter that influences vegetation growth and is impacted by vegetation itself. Regions with dense vegetation maintain a surface temperature below 35°C , preventing excessive heat accumulation. Extreme temperature deviations, whether too low or too high, negatively affect vegetation growth and disrupt the plant's phenological cycle. The study of Tian Shan's land surface temperature over a 23-year period reveals a range between 250.48 and 303.59 Kelvin (Fig. 8A). The highest average temperatures are observed in the northern and central regions. The abnormal slope value indicates a consistent average temperature across all areas of

Tian Shan, varying from 1.25 to -1.17 Kelvin (Fig. 8B). There is a minimal change in the trend of this variable throughout the statistical period, except for a significant increase in 2022 compared to previous years (Fig. 8C).

Temperature, along with sunlight availability and water supply, plays a crucial role in shaping global plant growth patterns, influencing the suitability of land for forests, grasslands, or deserts. This relationship is exemplified in the Tian Shan ecoregions, where the connection between 2-meter ground temperature and vegetation cover is scrutinized. The 23-year average temperatures in these regions reveal higher values in the northern, northeastern, and western areas, ranging from 259.03 to 285.4 Kelvin (Fig. 9A). Interestingly, the average anomalous slope remains relatively stable across the region except for a significant temperature drop in 2021, indicating consistent patterns over the years (Fig. 9B and C). This analysis highlights the intricate link between temperature and vegetation cover in the Tian Shan ecoregions, emphasizing the importance of temperature in shaping terrestrial ecosystems.

Actual Evapotranspiration (ETa) refers to the amount of water lost from a surface due to evaporation and transpiration. This measurement is expressed in millimeters and provides an estimate of the water requirement for actively growing plants. When vegetation is present, the surface holds more water, leading to higher water loss in the atmosphere, while wastelands experience more heat and stronger winds, resulting in less water to evaporate. The Tian Shan ecoregions have varying levels of ETa, with the central regions experiencing the highest amounts. This parameter has been decreasing from 2016 to 2021, with the anomaly slope being uniform for central, northern, and western regions, but the lowest values have been reported for the southwestern and eastern regions.

Trees are affected by winds, which impact transpiration, growth rate, and tree shape. Wind increases transpiration and water loss (Clark et al. 2000). Trees can also reduce wind speed. In the Tian Shan ecoregions, the southwest and west regions have the lowest average wind speed, while the southeast and east regions have the highest (Fig. 11A). The slope of wind speed changes is consistent throughout the area, considering the topography (Fig. 11B). The highest average wind speed was recorded in 2010, and the lowest was in 2018 (Fig. 11C).

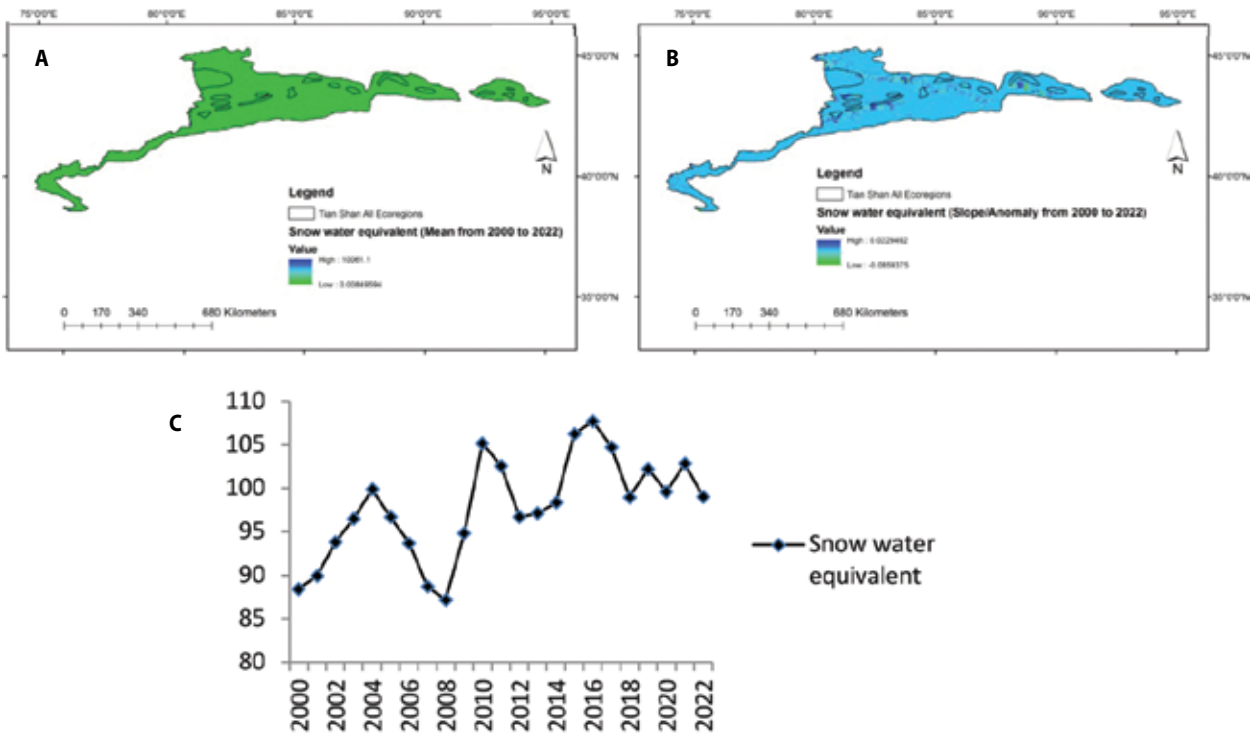


Figure 6. Changes in the snow-equivalent water mean (A), changes in the snow-equivalent water slop/anomaly (B), and average snowmelt changes in the Tian Shan ecological zone during the statistical period 2000–2022 (C)

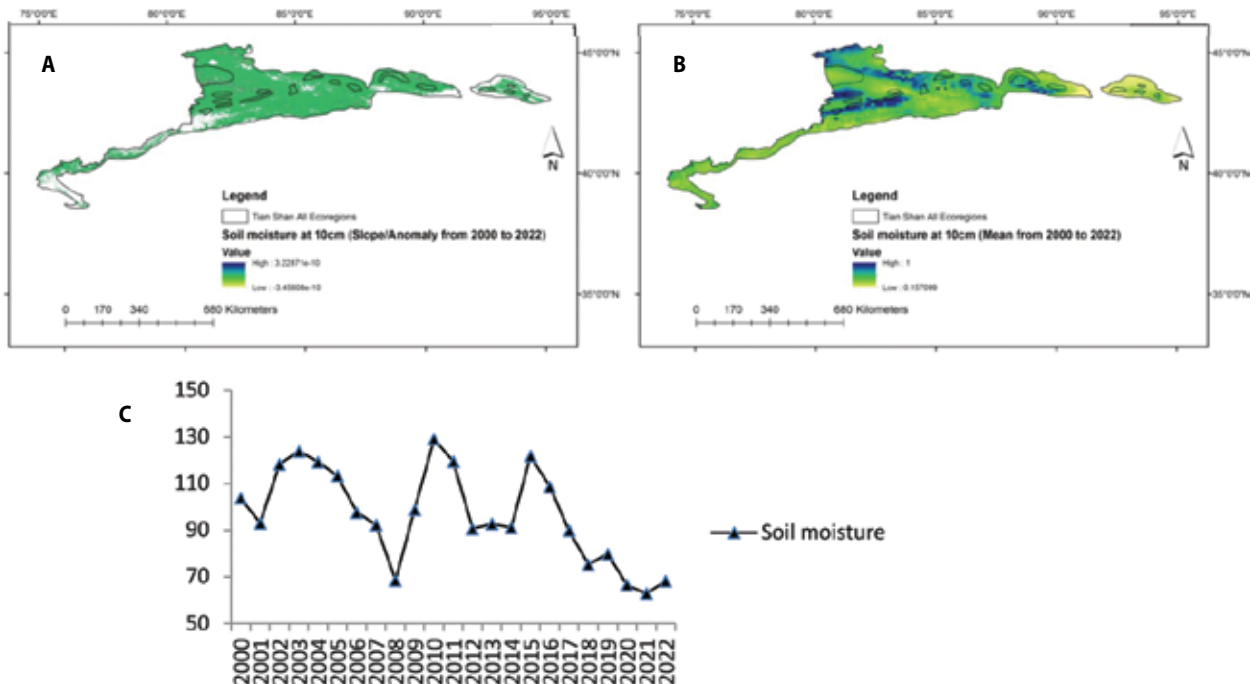


Figure 7. Changes in the soil moisture at 10 cm slop/anomaly (A), changes in the soil moisture at 10 cm mean (B), and changes in the average soil moisture content of Tian Shan area during the statistical period 2000–2022(C)

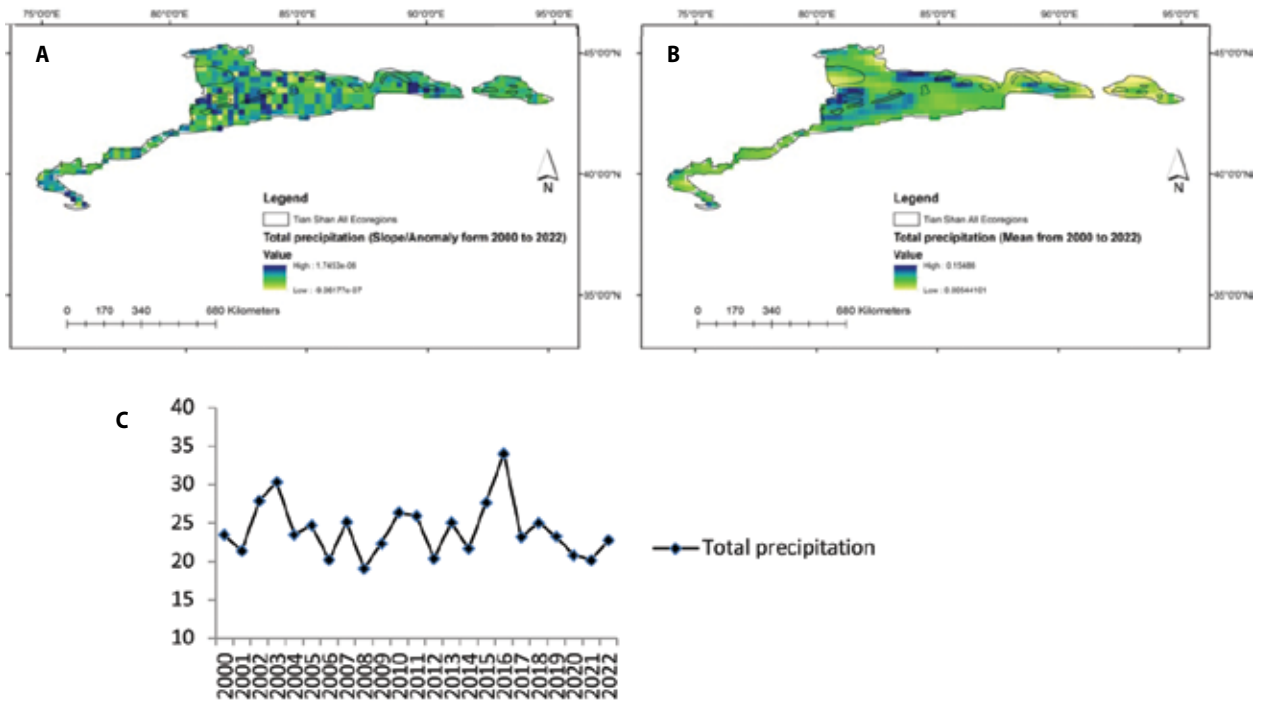


Figure 8. Changes in the LST daily time mean (A), changes in the LST daily time slop/anomaly (B), and changes in the average land surface temperature of the Tian Shan ecological zone during the statistical period 2000–2022 (C)

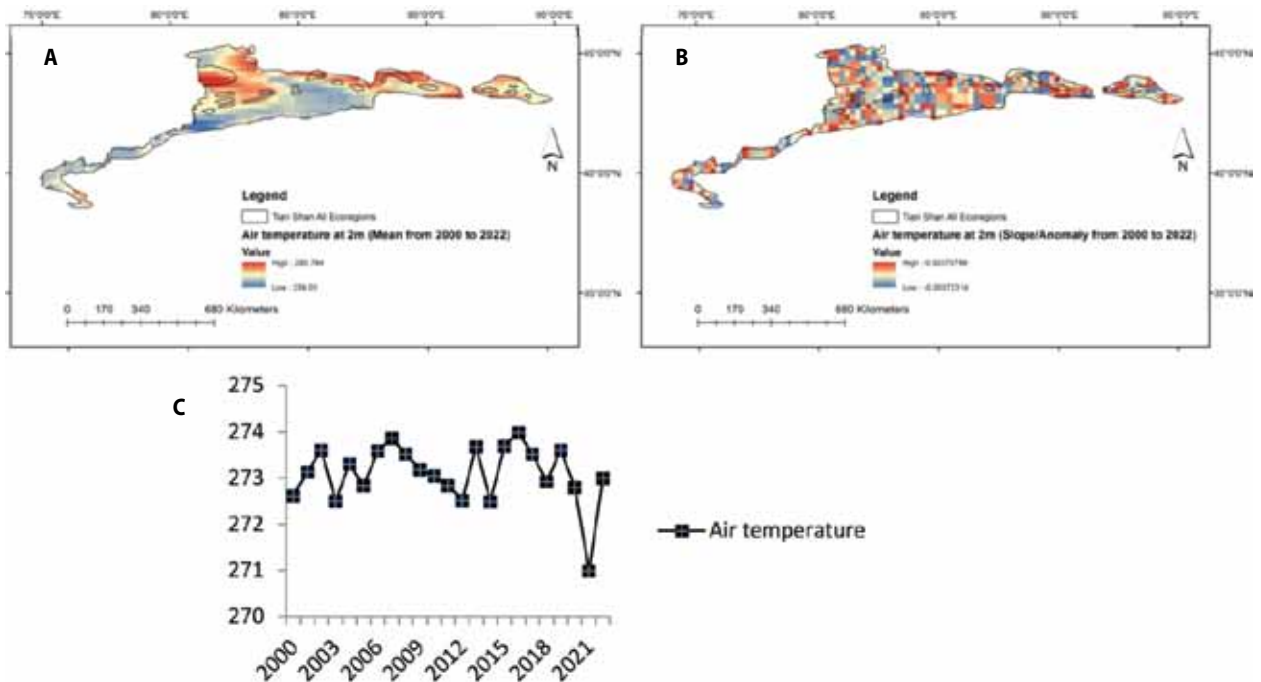


Figure 9. Changes in the air temperature at 2 m mean (A), changes in the air temperature at 2 m slop/anomaly (B), and changes in the average air temperature of the Tian Shan ecological zone during the statistical period 2000–2022 (C)

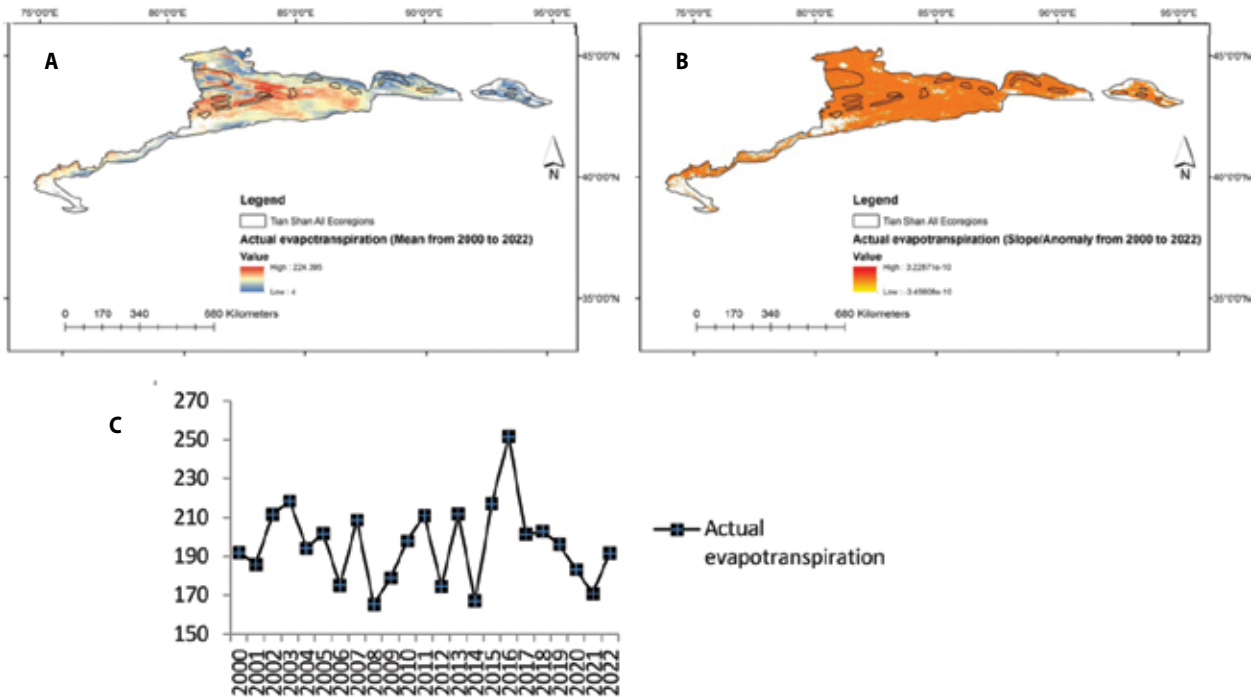


Figure 10. Changes in the actual evapotranspiration mean (A), changes in the actual evapotranspiration slop/anomaly (B), and changes in the mean actual evapotranspiration of Tian Shan ecoregion area during the statistical period 2000–2022 (C)

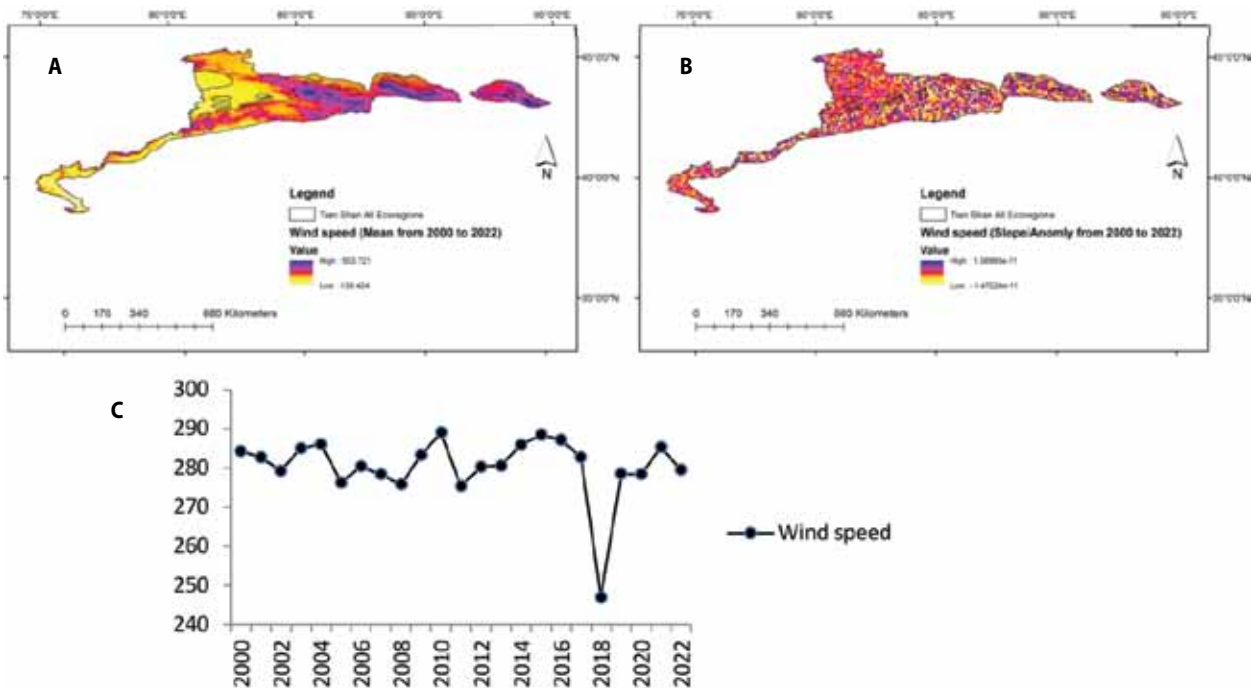


Figure 11. Changes in the wind speed mean (A), changes in the wind speed slop/anomaly (B), and changes in the average wind speed of the Tian Shan ecoregions during the statistical period of 2000–2022 (C)

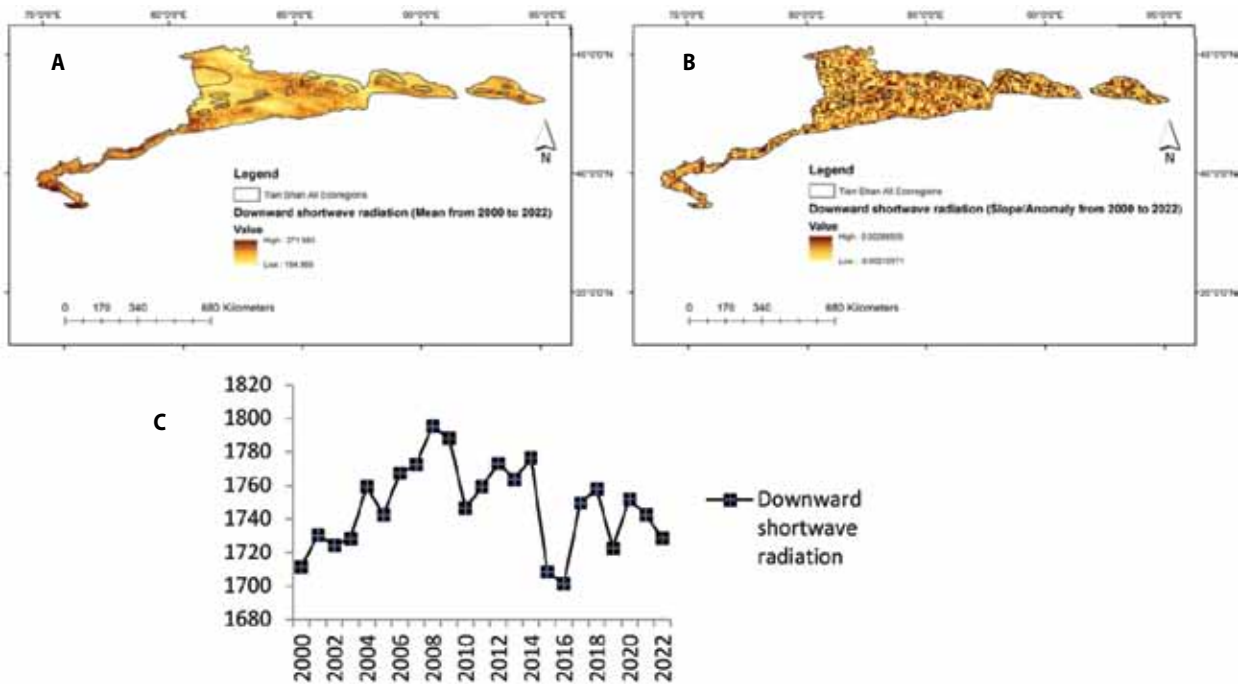


Figure 12. Changes in the downward shortwave radiation mean (A), changes in the downward shortwave radiation slope/anomaly (B), and changes in the average shortwave radiation of Tian Shan ecoregions during the statistical period of 2000–2022 (C)

Shortwave radiation is crucial for evaporation, transpiration, and photosynthesis in agricultural systems. In the Tian Shan ecoregion, the central and southwest areas receive higher levels of downward shortwave radiation, while the northern and northwest regions receive comparatively lower levels (Fig. 12A). Patterns of slope and anomalies in downward shortwave radiation are observed in all ecoregions (Fig. 12B). From 2006 to 2009, the highest amount of radiation was observed, but recent years (2020 to 2022) have shown a decreasing trend, reaching the lowest level (Fig. 12C).

Human drivers

Human parameters significantly influence vegetation growth in the Tian Shan ecological zone, as highlighted in the study. Notably, the Light Index and CNLI serve as key indicators of human presence and activities in the region, showing an increasing trend since 2000. In 2019, record-high levels were observed, with the Light Index and CNLI reaching 72% and 11%, respectively (Tab. 3).

The changes in CNLI percentages and average DMSP values are graphically depicted in column and circular charts, with the highest average DMSP recorded in 2019 (Fig. 13).

The study demonstrates the use of nighttime light data from DMSP to simulate human activity intensity and assess its impact on habitat quality, showcasing the feasibility of evaluating human activities’ effects

Table 3. Statistics related to human drivers from 2000 to 2020 using advanced sensors and night data extraction

Year	Mean value	Sum (S)	Total sum	Mean (zonal statistic)	Light index (%)	CNLI (%)
DMSP NTL 2000	0.2365	8,959	342,016	8.78	23	0.36
DMSP NTL 2005	0.3348	12,394	342,016	9.10	33	0.52
DMSP NTL 2010	0.5766	23,919	342,000	8.15	57	0.90
DMSP NTL 2015	1.7730	79,304	342,016	7.33	17	2.60
DMSP NTL 2018	3.9763	184,971	342,016	7.34	39	6.30
DMSP NTL 2019	7.2632	317,604	342,016	7.75	72	11.00
DMSP NTL 2020	2.1115	79,180	342,016	9.11	21	3.34

on habitat through such data on a global scale (Zhao et al. 2022). The spatial patterns of DMSP nighttime data from 2000 to 2020 in Tian Shan ecoregions are illustrated in Figure 14, indicating increasing human presence and activity over time. The study suggests a positive correlation between human indicators and plant indicators, showcasing the beneficial influence of human activities on vegetation development in the region. The average DMSP values ranged from 0 to 63, with higher values concentrated in the western, northern, and north-eastern areas of Tian Shan, correlating with increased vegetation cover and forestry activities. The study highlights the continuous expansion of human activity and its positive effects on vegetation in the area.

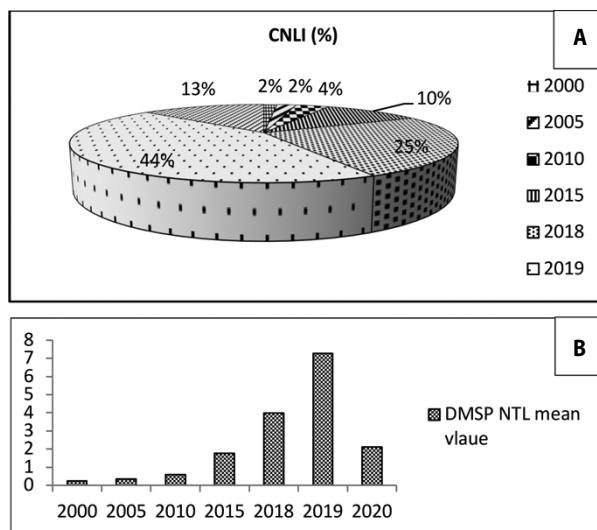


Figure 13. Chart of human parameter changes during the statistical period

The study depicted in Figure 15 presents 3D scatter plots analyzing the influence of climate, environmental factors, and human activities on NDVI and EVI in the Tian Shan ecoregions. These plots help in assessing data normality and visualizing the complex relationships between the variables. The X and Y axes represent the dependent variables (NDVI and EVI), while the Z axis represents independent variables capturing climatic, environmental, and human drivers. The research underscores that climatic and environmental parameters significantly impact vegetation in the Tian Shan ecoregions, with factors like precipitation, radiation, soil moisture, runoff, and temperature playing cru-

cial roles. The study utilized Pearson correlation and the Matrix network to establish these relationships, highlighting the key role of air temperature and wind speed in affecting NDVI and EVI in the region.

In a review of trends in 3D LST scattering graphs in Tian Shan ecoregions, it is noted that some data points have been excluded, causing oscillations in the data (Fig. 15). The relationship between LST and vegetation varies throughout the seasons, with a negative correlation in warm seasons and a positive correlation in cold seasons. The preservation of vegetation in Tian Shan winters over a 23-year period is attributed to radiation levels. Wind speed is identified as a factor leading to vegetation loss, showing a negative regression relationship with plant indicators. By utilizing 3D scatter plot models, researchers examine the relationship between vegetation indices, such as NDVI and EVI, with CNLI and DMSP in the Tian Shan ecoregions. The study finds a strong positive correlation (Pearson correlation coefficient >0.73) between these variables. Human presence in the region is linked to vegetation development, water and soil conservation efforts, and mitigation of soil erosion, contributing to the overall improvement of the ecosystem.

Correlation matrix

A correlation matrix is a tabular representation that displays correlation coefficients between different variables. Each cell in the matrix showcases the correlation between two specific variables. This matrix is utilized for summarizing data, serving as an input for more advanced analyses, and functioning as a diagnostic tool for advanced analytical processes (Tab. 4).

The study analyzed the correlation between various environmental parameters and vegetation indices NDVI and EVI. The results revealed that soil moisture had the most significant negative correlation effects on both NDVI (-0.58) and EVI (-0.57), followed by the wind speed with values of -0.30 and -0.32 , and DSR with an inverse correlation to vegetation. SWE and AEA showed weak associations with NDVI and EVI. Runoff had the least impact on the indices. Notably, precipitation and transpiration, as well as precipitation and runoff, exhibited the highest correlation values of 0.94 and 0.92, respectively. These findings highlight the complex interplay between environmental factors and vegetation health (Tab. 4).

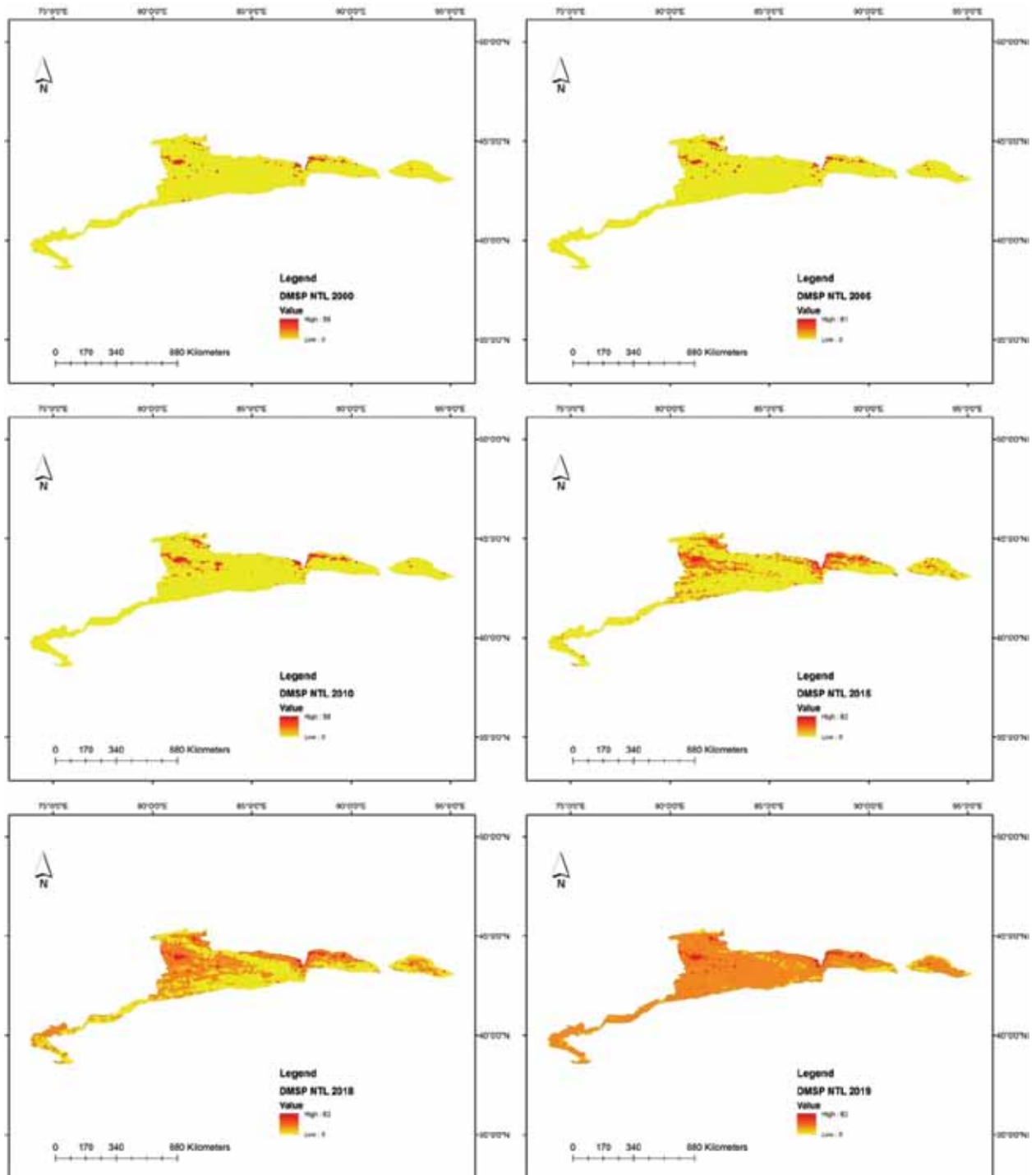


Figure 14. Effects of DMSP during different statistical periods from 2000 to 2019

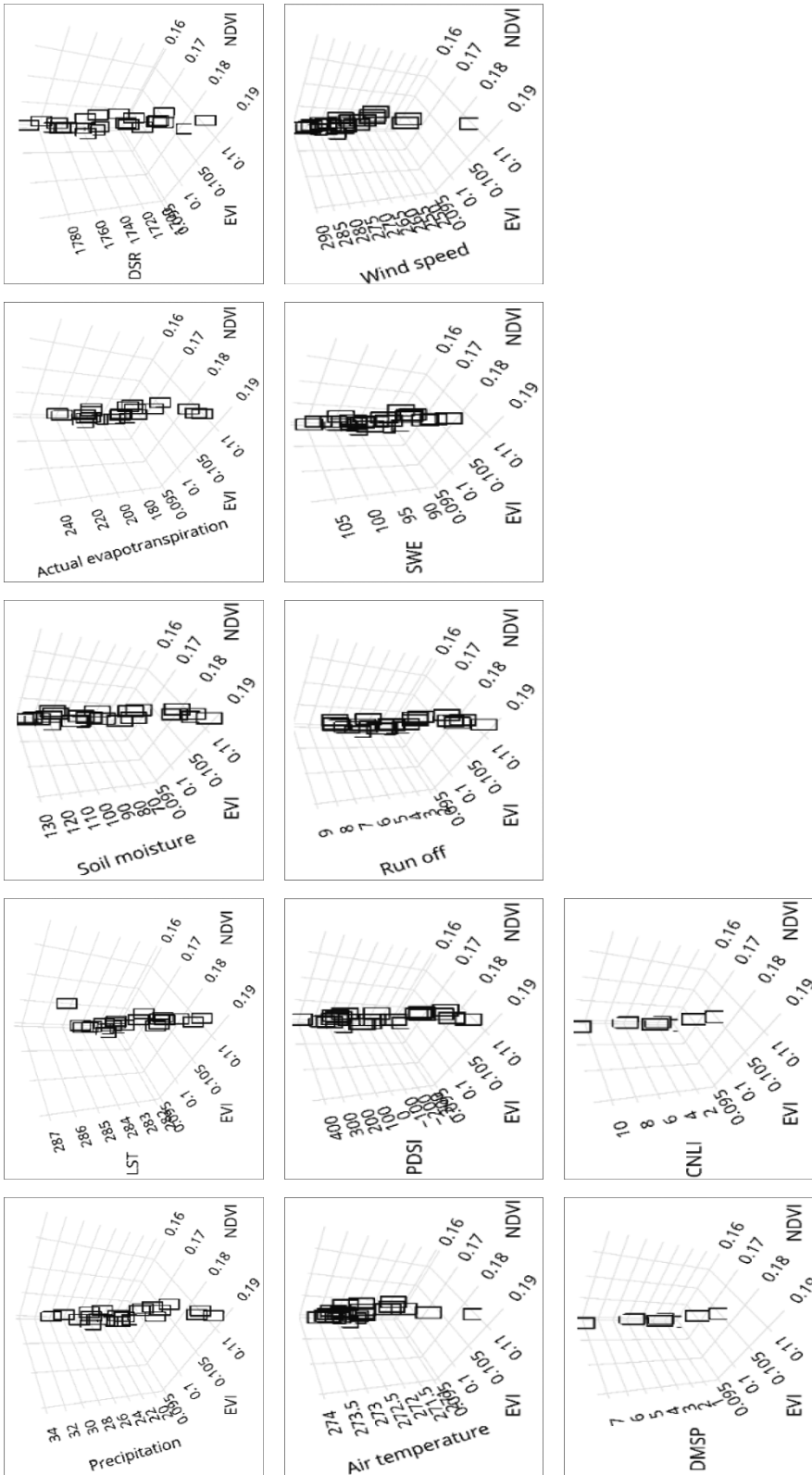


Figure 15. Three-dimensional diagram of the effects of climatic, environmental, and human parameters on the coverage of the Tian Shan ecological area

Table 4. Correlation matrix of climate parameters and environment and human drivers with vegetation indicators in Tian Shan ecoregions

Parameters	NDVI	EVI	LST	Total precipitation	Soil moisture	Actual evapotranspiration	DSR	Air temperature at 2 m	PDSI	Run off	Snow water equivalent	Wind speed
NDVI	1.0000											
EVI	0.9916	1										
LST	0.1906	0.220	1.000									
Total precipitation	0.0445	0.044	-0.310	1								
Soil moisture	-0.5839	-0.570	-0.540	0.6417	1.0000							
Actual evapotranspiration	0.2264	0.224	-0.260	0.9432	0.5336	1.0000						
DSR	-0.2708	-0.250	0.131	-0.5924	-0.2929	-0.6113	1					
Air temperature at 2 m	0.0356	0.033	0.078	0.3486	0.2616	0.4683	-0.06	1				
PDSI	-0.0959	-0.120	-0.490	0.7763	0.7336	0.7659	-0.58	0.2533	1.000			
Run off	0.0028	-0.010	-0.320	0.9294	0.7070	0.8968	-0.58	0.3969	0.849	1.0000		
Snow water equivalent	0.2833	0.244	-0.090	0.4135	0.1860	0.4148	-0.37	-0.0506	0.468	0.4471	1.0000	
Wind speed	-0.3068	-0.320	-0.040	0.1184	0.3789	0.0295	-0.25	-0.0102	0.207	0.2473	0.1736	1.0000

In the above matrix model, the numerical value of zero is determined in white, the numerical value of -1 in yellow, and the numerical value of +1 in blue, respectively.

The study conducted in the Tian Shan ecoregions reveals a significant positive correlation between human parameters and vegetation indicators, showcasing the impacts of human activities and climatic variables on vegetation dynamics. Table 5 presents the correlation analysis results, demonstrating that NDVI shows a strong positive correlation with human activity proxies CNLI (0.74) and DMSP (0.73), indicating a higher vegetation cover in areas with more human presence and intervention. In contrast, the relationship between EVI and human activity proxies is weaker. The study suggests that NDVI is more sensitive to detecting positive impacts of activities like vegetation restoration, pasture and watershed management, and soil conservation, leading to an expansion of vegetation cover in the region. The findings highlight that human activities have been a dominant driver of vegetation changes, surpassing the influences of climate, and environmental factors, emphasizing the increasing positive impact of human activities on vegetation development in the region over recent years. The matrix model illustrates a strong correlation between the vegetation indicators NDVI and EVI and key human drivers in the Tian Shan ecosystems, suggesting a link between human activities and ecosystem management initiatives like natural resource conservation, forestry, plantation activities, watershed vegetation restoration, ecotourism, and road construction to prevent seasonal fires. This highlights the significant influence of human interventions on the ecological balance in the area.

Table 5. Correlation matrix of human parameters and vegetation cover index of Tian Shan ecoregions

Parameters	EVI	NDVI	DMSP	CNLI
EVI	1			
NDVI	0.9940	1		
DMSP	0.7259	0.7388	1	
CNLI	0.7349	0.7480	0.9995	1

Pearson's correlation coefficient

The Pearson correlation coefficient (r) is a widely used method to measure linear correlations between two variables. It ranges from -1 to 1, indicating both the strength and direction of the relationship. The coefficient is appropriate when the relationship is linear, both variables are quantitative, they follow a normal distri-

bution, and there are no outliers. The correlation value also represents the effect size of the correlation. To interpret the effect size, Cohen’s guidelines (Cohen 1988) are often followed, as shown in Table 6.

Table 6. Correlation value and effect size

Correlation value (r)	Level
-1.0	Perfectly negative
-0.8	Strongly negative
-0.5	Moderately negative
-0.2	Weakly negative
0.0	No association
0.2	Weakly positive
0.5	Moderately negative
0.8	Strongly positive
1.0	Perfectly positive

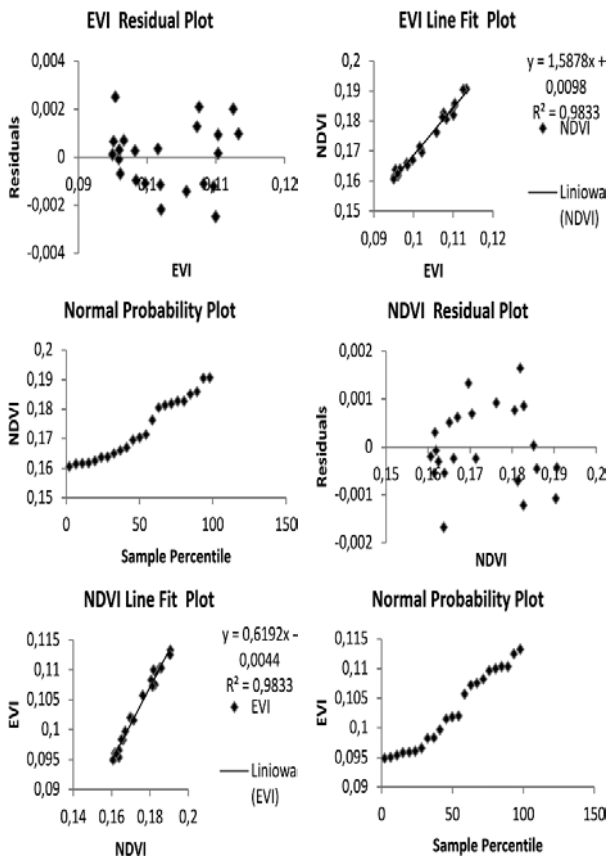


Figure 16. Normal distribution charts and residuals plots of NDVI and EVI in Tian Shan ecoregions

Pearson’s test was used to measure the correlation between vegetation indices (NDVI and EVI) and climate parameters and environmental and human drivers in Tian Shan ecoregions. Before applying the test, data normality was checked and confirmed (Fig. 16). The test results indicate a significant correlation between variables when the P-value is less than 0.05 (95% level) and the correlation coefficient (r) measures the influence of parameters. Additionally, residual plots were used to assess homogeneity of variance and detect outliers ($>\pm 3$). Linear regression was employed to determine the best-fitting line, enabling prediction of output values based on given inputs. Normal probability plots were used to assess normality of the dependent variable data (5).

Correlation between NDVI and EVI

Pearson correlation coefficient showed that NDVI and EVI are perfectly related together with a value of 0.991 (Tab. 7) in Tian Shan ecoregions, although NDVI is very common to calculate vegetation and EVI is much more sensitive to atmospheric errors and is suitable for dense covers.

Table 7. Pearson correlation between vegetation indices

Parameter	Value
Pearson correlation coefficient (r)	0.991
P-value	0.000
Covariance	0.000
Sample size (n)	23.000
Statistic	35.122

Correlation between climatic and environmental parameters with NDVI and EVI

The study conducted in the Tian Shan ecoregions explored the relationship between the NDVI and EVI indices with various climate and environmental parameters, emphasizing the significant correlation with soil moisture (Fig. 17 and 18). Tables 8 and 9 provided a clear indication of the values and effectiveness of these relationships. The analysis revealed a strong negative correlation (Pearson coefficients of -0.58 for NDVI and -0.57 for EVI) between vegetation indicators and soil moisture, suggesting that as soil moisture increases, vegetation indicators decrease due to water-filled stress and saturated soil conditions caused by factors like

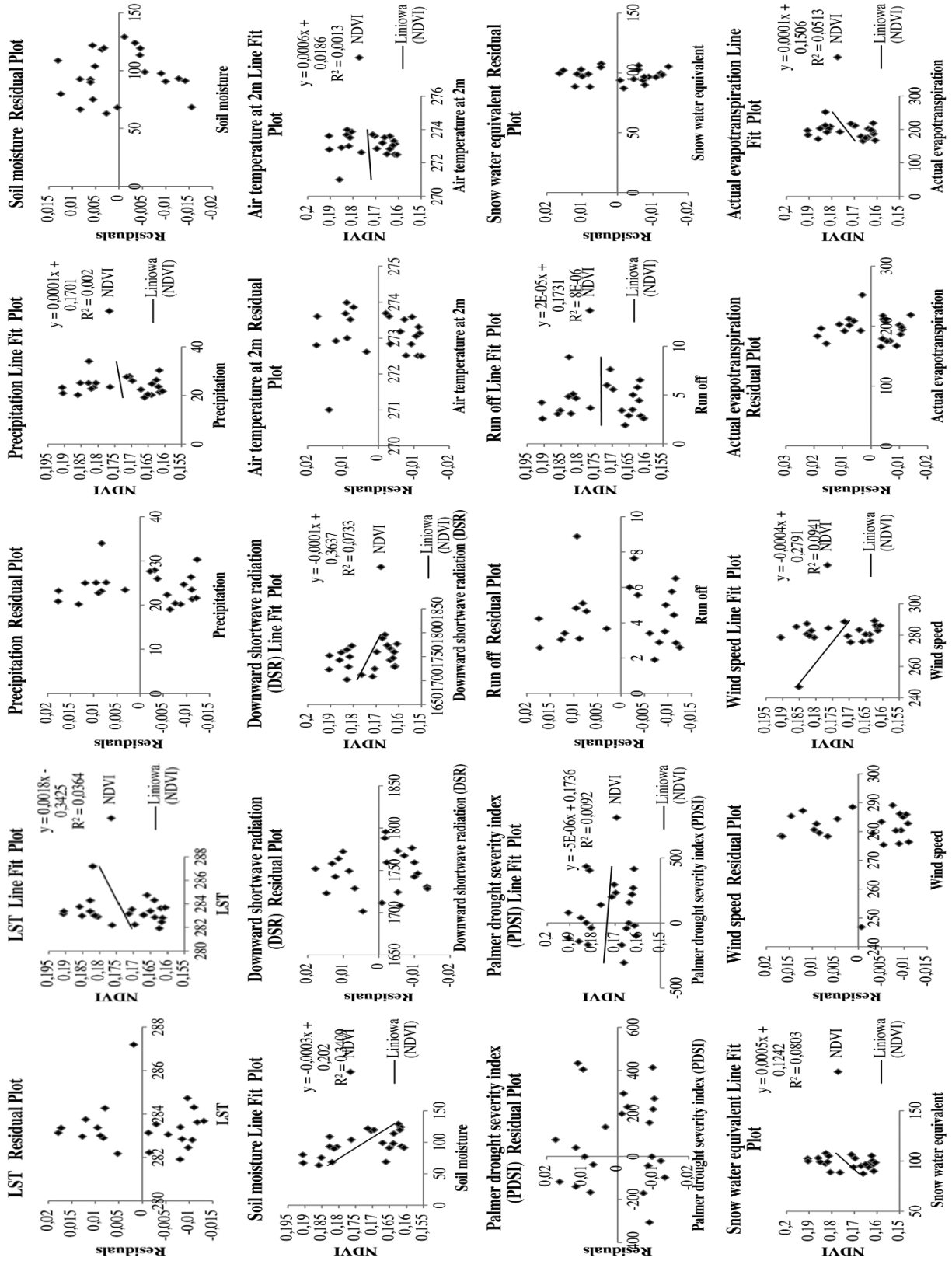


Figure 17. Correlation between climate and environmental variables with NDVI

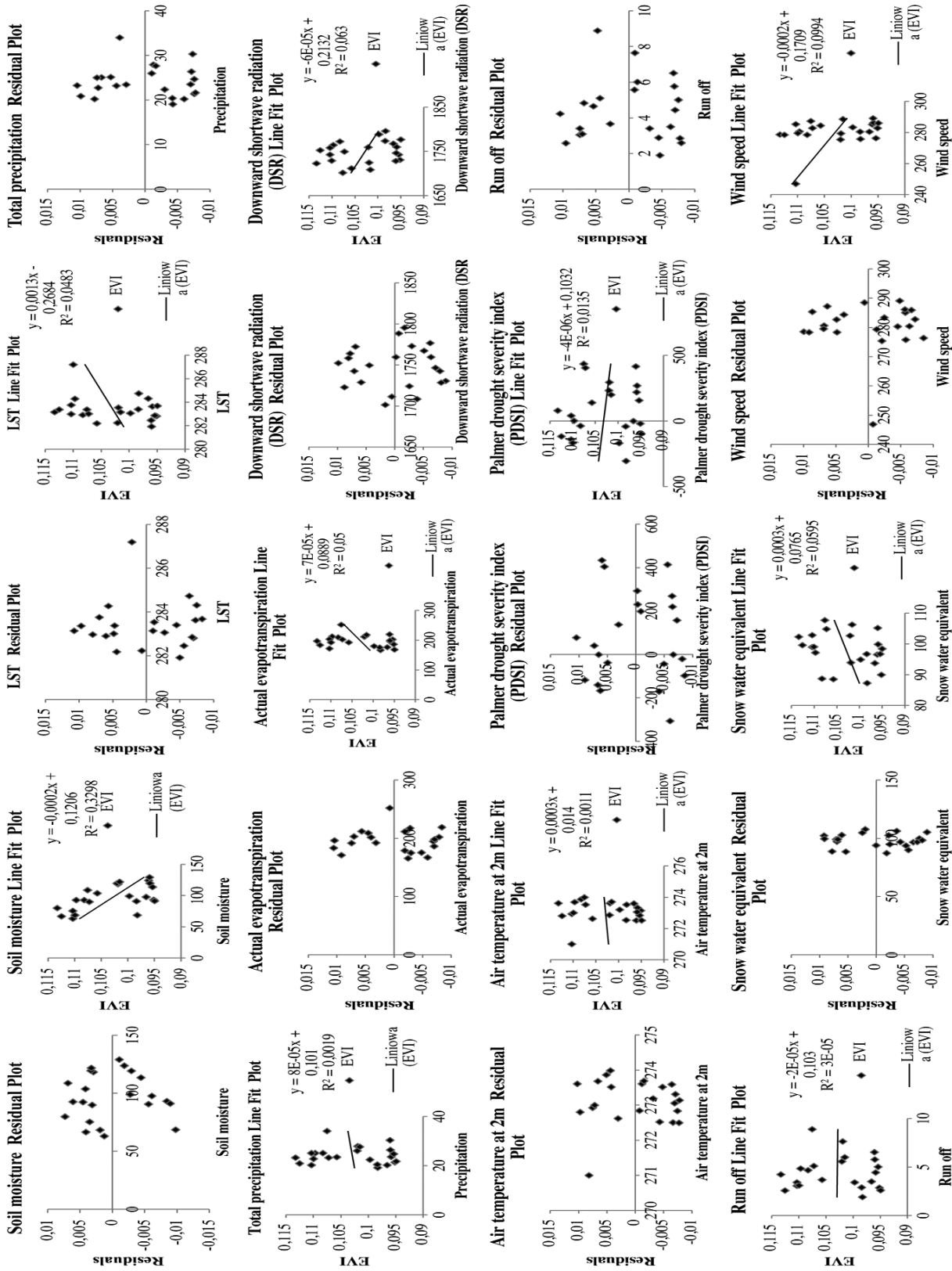


Figure 18. Correlation between climate and environmental variables with EVI

swamps, rivers, lakes, and snow-covered mountains. The findings underscored the impact of seasonal variations, particularly in the cold seasons, on hindering vegetation growth in the region.

The Pearson regression model indicated weak-to-typical correlations between NDVI and EVI with DSR parameters of -0.277 and -0.251 , showcasing a negative relationship with the wind speed as well ($r = -0.306$ and -0.315) as shown in Tables 8 and 9. The negative impact of DSR and wind speed on plant development and growth elucidates these associations. Conversely, Snow Water Equivalent and Actual Evapotranspiration parameters displayed relatively weak to normal positive correlations with NDVI and EVI ($r = 0.283, 0.243, 0.226, 0.223$), while the LST index exhibited an abnormal relationship with the plant indices. However, the remaining precipitation and temperature parameters, PDSI drought index, and runoff demonstrated weak connections with NDVI and EVI, prompting further discussion and analysis in this area (Tab. 8 and 9).

Table 8. Relationship between climate and environmental variables with NDVI using Pearson regression model

	Parameters	P-value	r	Covariance	T	N
NDVI	LST	0.380	0.190	0.002	0.089	23
	Total precipitation	0.840	0.044	0.001	0.089	
	Soil moisture	0.003	-0.588	-0.121	-3.299	
	DSR	0.211	-0.277	-0.070	-1.289	
	Air temperature at 2 m	0.871	0.035	0.000	0.163	
	PDSI	0.663	0.095	-0.202	-0.441	
	Runoff	0.989	0.002	0.000	0.013	
	Snow water equivalent	0.190	0.283	0.016	1.353	
	Wind speed	0.154	-0.306	-0.026	-1.447	
	Actual evapotranspiration	0.298	0.226	0.046	1.065	

The vegetation patterns in a region are strongly influenced by environmental factors which have experienced significant fluctuations between dry and wet conditions over time, leading to the current vegetation distribution observed amidst substantial environmental changes (Wang et al. 2005). These interactions between

vegetation and environmental factors occur at different temporal scales, with intricate and nonlinear relationships especially prevalent at a regional level (Zhang et al. 2018). The distribution of vegetation types like mountain steppe, seasonal grassland, common steppe, and desert steppe within the region is largely shaped by soil moisture factors, with human activities at a local scale potentially contributing to vegetation changes as well (Shao et al. 2018). Moreover, non-climatic environmental alterations, including variations in soil moisture levels, can impact the correlation between NDVI and EVI, highlighting the need to account for uncertainties when predicting NDVI responses to future changes (Li-ang and Yang 2016; Pei et al. 2019).

Table 9. Relationship between climate and environmental variables with EVI using Pearson regression model

	Parameters	P-value	r	Covariance	T	N
EVI	LST	0.311	0.219	0.000	1.023	23
	Total precipitation	0.840	0.043	0.000	0.201	
	Soil moisture	0.003	-0.577	-0.074	-3.021	
	DSR	0.247	-0.251	-0.041	-1.185	
	Air temperature at 2m	0.188	0.032	0.000	0.150	
	PDSI	0.597	0.116	-0.153	-0.536	
	Runoff	0.979	0.055	0.000	0.155	
	Snow water equivalent	0.262	0.243	0.009	1.152	
	Wind speed	0.142	-0.315	-0.016	-1.522	
	Actual evapotranspiration	0.305	0.223	0.038	1.051	

The study revealed a strong correlation between the vegetation indices NDVI and EVI, indicating that they share similarities. Factors such as wind speed, snow water equivalent, DSR, and soil moisture were identified as impactful on these indicators in various alignments. EVI was recognized for its ability to consider atmospheric conditions and reduce canopy background noise, showing higher sensitivity in densely vegetated regions compared to NDVI. The average NDVI over the 23-year period was 0.173, with values ranging from -1.0 to 1.0 indicating different land cover types. The Tian Shan ecoregion exhibited sparse vegetation. Further

analysis revealed the relationships between EVI and the environmental driver parameters as follows:

Correlation between human activities and NDVI and EVI

Results of the Pearson correlation indicated that there is a large positive (Relatively strong) relationship between NDVI and DMSP, ($r(5) = 0.738$, $p = 0.048$), and a large positive relationship between NDVI and CNLI, ($r(5) = 0.748$, $p = 0.043$) (Tab. 10).

Table 10. Pearson correlation between NDVI and mean DMSP

Parameter	DMSP	CNLI
Pearson correlation coefficient (r)	0.73800	0.748
P-value	0.04800	0.043
Covariance	0.02241	0.034
Sample size (n)	7	7
Statistic	2.45100	2.520

Plant indicators in Tian Shan ecoregions show a unique relationship with human presence. Contrary to the expected negative impact of human activities on vegetation cover, it is found that human presence can have a positive and closely related effect on plant indicators in the area. The model suggests that efforts should be directed toward conserving, enhancing, and sustainably utilizing biological resources and the global ecological heritage in these ecoregions.

Anomalies and changes in vegetation cover in time series 2000–2022

Over a span of 23 years, from 2000 to 2022, the study analyzed and represented the anomalies and transformations in vegetation within the Tian Shan Ecoregions. The findings illustrated in Table 11 and Figure 19 present the extent and ratios of deforestation, afforestation, unchanged vegetation areas, and regions targeted for vegetation rehabilitation efforts. The study indicated that deforestation and vegetation reduction only increased by 3% covering 7190.119633 square kilometers, whereas afforestation activities demonstrated significant growth by 6%, expanding over 12,089.28333 square kilometers. Additionally, a considerable portion of the Tian Shan ecoregions, accounting for 36% with 78,733.91197 square kilometers, maintained unchanged

vegetation cover, while 55% with 120,032.6253 square kilometers remained devoid of vegetation.

Table 11. Vegetation anomalies and changes during the period from 2000 to 2022

Description of the changes	Area (km ²)
No vegetation (unchanged)	120,032.63
Deforestation	7,190.12
Afforestation	12,089.28
Vegetation (unchanged)	78,733.91

According to studies conducted by Li et al. (2020) and Q. Wang et al. (2020), the implementation of the Grain to Green project in Southwest China has contributed to the growth of vegetation. This positive trend has been observed not only in Southwest China but also in various regions across the country, leading to a significant increase in forested areas.



Figure 19. Anomaly and changes in vegetation area during the period 2000–2022

Anomalies and changes in land-use and land cover in the time series 2001–2021

To monitor land-use changes and land cover in the Tian Shan ecoregion, which denotes physical land types like forests or open water, we analyze how resources and land are utilized. By assessing data and land cover maps over time, ecological managers can track land-use patterns and alterations. The study will integrate land cover details for various essential purposes such as evaluating non-point sources of pollution, comprehending landscape variables for environmental analysis, assessing chemical behaviors, and analyzing air pollution impacts

The finding of LULC prediction for 2001

In 2001, the Tian Shan region exhibited distinct land-use and land cover (LULC) classifications. The smallest area was occupied by Evergreen Needleleaf Forests, covering 41.51 square kilometers and dominated by evergreen conifer trees, while the largest area belonged to Grasslands spanning 142,376.597 square kilometers with herbaceous annuals. Grasslands predominantly covered the northwest, central, and northeast regions, forming barren areas in the southwest and southeast. The barren areas were characterized by desert conditions with minimal water and dry grass. Croplands were prevalent in central regions, while the western parts were rich in coniferous and broad-leaved forests, contributing significantly to the biological balance within the Tian Shan ecoregions. These land cover types, along with barren lands and croplands, constituted the primary classifications in the LULC, comprising 65.28%, 25.43%, and 7.7% of the total area in 2001. The diverse LULC patterns in the Tian Shan region play a crucial role in supporting plant and animal species richness, carbon fixation cycles, microcli-

mate improvements, and overall biological stability within the ecoregions (Tab. 12, Fig. 20).

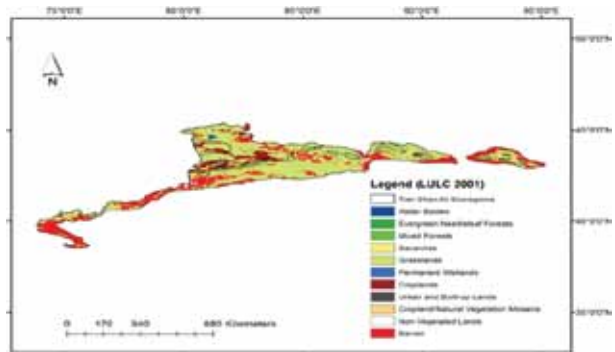


Figure 20. Visual pattern and classifications of LULC in 2001 in Tian Shan ecoregions

The finding of LULC prediction for 2021

In 2021, the Tian Shan ecoregions database revealed the dominance of grasslands spanning 145,028.7926 square kilometers, representing 66.54% of the total

Table 12. Area and percentage and classifications of LULC

Value	Description (LULC 2001)	Year 2001		Year 2021	
		area (km ²)	percent	area (km ²)	percent
0	Water bodies: at least 60% of area is covered by permanent water bodies	554.99	0.25	563.78	0.250
1	Evergreen Needleleaf Forests: dominated by evergreen conifer trees (canopy >2m). Tree cover >60%.	41.51	0.01	21.05	0.009
5	Mixed Forests: dominated by neither deciduous nor evergreen (40–60% of each) tree type (canopy >2m). Tree cover >60%	248.60	0.11	173.45	0.070
9	Savannas: tree cover 10–30% (canopy >2m)	334.55	0.15	102.25	0.040
10	Grasslands: dominated by herbaceous annuals (<2 m)	142,376.59	65.28	506.15	0.230
11	Permanent wetlands: permanently inundated lands with 30–60% water cover and >10% vegetated cover	344.95	0.15	145,028.79	66.540
12	Croplands: at least 60% of area is cultivated cropland	16,810.66	7.70	83.62	0.030
13	Urban and built-up lands: at least 30% impervious surface area including building materials, asphalt, and vehicles	92.25	0.04	17,376.65	7.970
14	Cropland/natural vegetation mosaics: mosaics of small-scale cultivation 40–60% with natural tree, shrub, or herbaceous vegetation	40.74	0.01	61.50	0.020
15	Non-vegetated lands: at least 60% of area is non-vegetated barren (sand, rock, soil) or permanent snow and ice with less than 10% vegetation	1,754.22	0.80	156.22	0.070
16	Barren: at least 60% of area is non-vegetated barren (sand, rock, soil) areas with less than 10% vegetation	55,469.53	25.43	2,368.31	1.080

area (Tab. 13), characterized by herbaceous annuals. In contrast, the Evergreen Needleleaf Forests comprised a mere 0.009% of the ecoregions, covering around 21.055089 square kilometers, with over 60% tree cover and exceeding 2 meters in canopy height. Croplands and barren areas accounted for 7.97% and 23.62%, respectively, showcasing significant land-use diversity. The landscape analysis depicted grasslands mostly in central and northern Tian Shan, barren desert regions in the south and southwest, and sporadic broadleaf coniferous forests. Farmlands were prominent in central regions, while other unique classifications added to the visual richness of the ecoregions. This LULC pattern analysis is summarized in Table 12 and visualized in Figure 21.

The term “Top Three classes” is used in the graphs because these three classes have the highest area ratio and percentage in land-use in 2001 and 2021. The term “Other Unique Classes” refers to ecological reserves and World Heritage sites. One example is the Tian Shan montane conifer forests, which consist of two main forest types: “Evergreen Needleleaf Forests” dominated by evergreen conifer trees with a tree cover exceeding 60%, and “Mixed Forests” with a balance of deciduous and evergreen trees (40–60% of each type) and a tree cover exceeding 60%. From 2001 to 2021, the coniferous community has decreased in extent, while the mixed broadleaf and coniferous community has expanded. The coniferous forest area reduced from 41.5 to 21 square kilometers, while the mixed forest area increased from 248.6 to 173.4 square kilometers.

The Tian Shan ecoregion is a bio-reserve estimated to have a life span of 2.5–7 million years (Carpenter 2000; Su et al. 2007). It is home to unique species such as the endemic karelini subspecies of Argali and Siberian Ibex, as well as endangered species like the Snow leopard. The region also supports dispersed populations of carnivores such as the gray wolf and Himalayan brown bear. Breeding populations of various bird species, including black stork, golden eagle, Houbara bustard, and bearded vulture, are found in Tian Shan. Conservation efforts are ongoing to monitor and protect these species and their habitats. Measures such as monitoring grazing activity, promoting wildlife connectivity, cross-border conservation opportunities, and studying the impacts of climate change on ecosystem cycles can help preserve the region’s biodiversity.

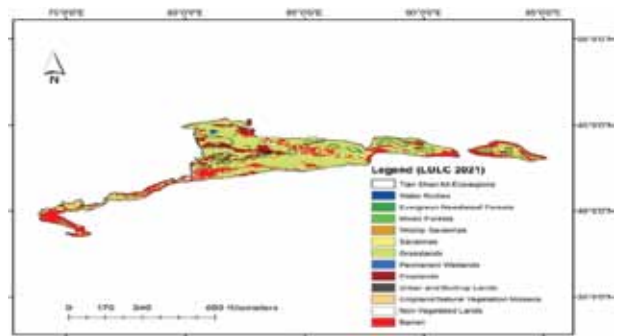


Figure 21. Visual pattern and classifications of LULC in 2021 in Tian Shan ecoregions

CONCLUSIONS

The study aims to understand the spatial patterns of vegetation dynamics in the vulnerable Tian Shan ecoregions and forecast the impact of future climate change on vegetation. The research explores the influences of human activities, climate conditions, geographical factors, and environmental impacts on vegetation. The results indicate the presence of healthy vegetation in the region, which is attributed to human presence and activities. NDVI and EVI indicators show positive trends, suggesting afforestation. There is a positive correlation between NDVI and human activities, as well as climatic and environmental parameters. However, a negative correlation is observed between NDVI/EVI and soil moisture due to high-altitude complications and freezing phenomena. The study emphasizes the importance of preserving and supporting unique ecosystems in the region. Overall, the findings highlight the dual role of positive human performance and constructive activities in mitigating the effects of unpredictable climate and environmental factors on vegetation in the Tian Shan ecoregions.

ACKNOWLEDGEMENTS

This research was supported by Xinjiang Institute of Ecology and Geography, Chinese Academy of Sciences, Urumqi, China; Tianchi Talents Project of Xinjiang (E3350107); National Natural Science Foundation of China (No. 42107084); and Key Research and Development Program of Xinjiang (2022B01032-4). A spe-

cial gratitude to Professor YU Ruide for providing insight, support, and expertise that greatly assisted the research.

REFERENCES

- Braswell, B.H., Schimel, D.S., Linder, E., Moore Iii, B. 1997. The response of global terrestrial ecosystems to interannual temperature variability. *Science*, 278 (5339), 870–873.
- Cao, K., Gao, J. 2022. Assessment of climatic conditions for tourism in Xinjiang, China. *Open Geosciences*, 14, 382–392.
- Cheng, J., Liang, S. 2018. Land-surface emissivity. In: Comprehensive remote sensing (ed. S. Liang). Elsevier, Oxford, 217–263. DOI: 10.1016/B978-0-12-409548-9.10374-4.
- Clark, A.J., Landolt, W., Bucher, J.B., Strasser, R.J. 2000. How wind affects the photosynthetic performance of trees: quantified with chlorophyll a fluorescence and open-top chambers. *Photosynthetica*, 38, 349–360.
- Cohen, J. 1988. Statistical power analysis for the behavioral sciences. Lawrence Erlbaum Associates Publishers, Hillsdale, NJ.
- Deng, H., Chen, Y. 2017. Influences of recent climate change and human activities on water storage variations in Central Asia. *Journal of Hydrology*, 544, 46–57.
- Deng, Y. et al. 2020. Spatiotemporal dynamics of soil moisture in the karst areas of China based on reanalysis and observations data. *Journal of Hydrology*, 585, 124744.
- Eastman, J.R., Sangermano, F., Machado, E.A., Rogan, J., Anyamba, A. 2013. Global trends in seasonality of normalized difference vegetation index (NDVI), 1982–2011. *Remote Sensing*, 5 (10), 4799–4818.
- Ecoregion data website. <https://ecoregions.appspot.com/>; <https://www.oneearth.org/>.
- Ehsanul, B., Nusrat, J.N., Bishal, R. 2021. Association of vegetation indices with atmospheric and biological factors using MODIS time series products. *Environmental Challenges*, 5, 100376.
- Fyfe, R. 2023. Human impact on vegetation. In: Handbook of archaeological sciences (eds. A.M. Pollard, R.A. Armitage, C.A. Makarewicz). John Wiley and Sons Ltd., 715–729. DOI: 10.1002/9781119592112.ch36.
- Gao, W. et al. 2022. NDVI-based vegetation dynamics and their responses to climate change and human activities from 1982 to 2020: A case study in the Mu Us Sandy Land, China. *Ecological Indicators*, 137, 108745.
- Gao, X., Huang, X., Lo, K., Dang, Q., Wen, R. 2021. Vegetation responses to climate change in the Qilian Mountain Nature Reserve, Northwest China. *Global Ecology and Conservation*, 28, e01698.
- Guo, E. et al. 2021. NDVI indicates long-term dynamics of vegetation and its driving forces from climatic and anthropogenic factors in Mongolian Plateau. *Remote Sensing*, 13 (4), 688.
- Hu, Y.F., Dao, R., Hu, Y. 2019. Vegetation change and driving factors: Contribution analysis in the Loess Plateau of China during 2000–2015. *Sustainability*, 11 (5), 1320.
- Jiapaer, G., Liang, S., Yi, Q., Liu, J. 2015. Vegetation dynamics and responses to recent climate change in Xinjiang using leaf area index as an indicator. *Ecological Indicators*, 58, 64–76.
- Jing, X., Yao, W.-Q., Wang, J.-H., Song, X.-Y. 2011. A study on the relationship between dynamic change of vegetation coverage and precipitation in Beijing's mountainous areas during the last 20 years. *Mathematical and Computer Modelling*, 54 (3/4), 1079–1085.
- Kottek, M., Grieser, J., Beck, C., Rudolf, B., Rubel, F. 2006. World Map of Koppen-Geiger Climate Classification Updated (PDF). Gebrüder Borntraeger. Retrieved September 14, 2019.
- Li, D., Wu, S., Liang, Z., Li, S. 2020. The impacts of urbanization and climate change on urban vegetation dynamics in China. *Urban Forestry and Urban Greening*, 54, 126764.
- Liang, P., Yang, X. 2016. Landscape spatial patterns in the Maowusu (Mu Us) Sandy Land, northern China and their impact factors. *Catena*, 145, 321–333.
- Liu, Y., Lei, H. 2015. Responses of natural vegetation dynamics to climate drivers in China from 1982 to 2011. *Remote Sensing*, 7 (8), 10243–10268.
- Liu, Y., Li, L., Chen, X., Zhang, R., Yang, J. 2018. Temporal-spatial variations and influencing factors of vegetation cover in Xinjiang from 1982 to 2013

- based on GIMMS-NDVI3g. *Global and Planetary Change*, 169, 145–155.
- Lovland, T., Merchant, J. 2004. Ecoregions and ecoregionalization: geographical and ecological perspectives. *Environmental Management*, 34, 1–13. DOI: 10.1007/s00267-003-5181-x.
- Luo, M. et al. 2019. Identifying climate change impacts on water resources in Xinjiang, China. *Science of the Total Environment*, 676, 613–626.
- Meredith, R.B., Jens, C.S. 2018. Human paths have positive impacts on plant richness and diversity: A meta-analysis. *Ecology and Evolution*, 8 (22), 11111–11121.
- Mihretab, G.G., Taibao, Y.B., Xuemei, Y., Temesghen, E.S. 2020. Assessment of NDVI variations in responses to climate change in the Horn of Africa. *The Egyptian Journal of Remote Sensing and Space Sciences*, 23, 249–261.
- Nemani, R.R. et al. 2003. Climate-driven increases in global terrestrial net primary production from 1982 to 1999. *Science*, 300 (5625), 1560–1563.
- Pei, Z. et al. 2019. The relationship between NDVI and climate factors at different monthly time scales: a case study of grasslands in inner Mongolia, China (1982–2015). *Sustainability*, 11 (24), 7243.
- Piao, S., Wang, X., Ciais, P., Zhu, B., Wang, T., Liu, J. 2011. Changes in satellite-derived vegetation growth trend in temperate and boreal Eurasia from 1982 to 2006. *Global Change Biology*, 17, 3228–3239.
- Rull, V., González-Sampériz, P., Corella, J.P., Morellón, M., Giralt, S. 2011. Vegetation changes in the southern Pyrenean flank during the last millennium in relation to climate and human activities: the Montcortès lacustrine record. *Journal of Paleolimnology*, 46, 387–404.
- Shi, S. et al. 2021. Quantitative contributions of climate change and human activities to vegetation changes over multiple time scales on the Loess Plateau. *Science of the Total Environment*, 755 (2), 142419.
- Shang, J. et al. 2022. Climate change drives NDVI variations at multiple spatiotemporal levels rather than human disturbance in Northwest China. *Environmental Science and Pollution Research*, 29 (10), 13782–13796.
- Shao, Y. et al. 2018. Relating historical vegetation cover to aridity patterns in the greater desert region of northern China: Implications to planned and existing restoration projects. *Ecological Indicators*, 89, 528–537.
- Sharma, M., Bangotra, P., Gautam, A.S., Gautam, S. 2022. Sensitivity of normalized difference vegetation index (NDVI) to land surface temperature, soil moisture and precipitation over district Gautam Buddha Nagar, UP, India. *Stochastic Environmental Research and Risk Assessment*, 36, 1779–1789.
- Shen, X., Liu, B., Zhou, D. 2016. Using GIMMS NDVI time series to estimate the impacts of grassland vegetation cover on surface air temperatures in the temperate grassland region of China. *Remote Sensing Letters*, 7 (3), 229–238.
- Sun, R., Chen, S., Su, H. 2021. Climate dynamics of the spatiotemporal changes of vegetation NDVI in northern China from 1982 to 2015. *Remote Sensing*, 13 (2), 187.
- Sun, Y., Yang, Y., Zhang, L., Wang, Z. 2015. The relative roles of climate variations and human activities in vegetation change in North China. *Physics and Chemistry of the Earth, Parts A/B/C*, 87/88, 67–78.
- Tucker, C.J. 1979. Red and photographic infrared linear combinations for monitoring vegetation. *Remote Sensing of Environment*, 8 (2), 127–150.
- Wang, S., Yang, B., Yang, Q., Lu, L., Wang, X., Peng, Y. 2016. Temporal trends and spatial variability of vegetation phenology over the Northern Hemisphere during 1982–2012. *PLoS One*, 11 (6), 0157134.
- Wang, Q., Li, Y., Luo, G. 2020. Spatiotemporal change characteristics and driving mechanism of slope cultivated land transition in karst trough valley area of Guizhou Province, China. *Environmental Earth Sciences*, 79, 1–18.
- Wang, X., Chen, F.H., Dong, Z., Xia, D. 2005. Evolution of the southern Mu Us Desert in North China over the past 50 years: an analysis using proxies of human activity and climate parameters. *Land Degradation and Development*, 16 (4), 351–366.
- Wei, Y., Liu, H., Song, W., Yu, B., Xiu, C. 2014. Normalization of time series DMSP-OLS nighttime light images.
- Wenbo, Z., Suhua, F., Baoyuan, L. 2001. Error assessment of visual estimation plant coverage. *Journal-Beijing Normal University Natural Science Edition*, 37 (3), 402–408.

- World Wildlife Federation (WWF). 2019. Available at <https://www.worldwildlife.org/> (access on 28 December 2019).
- Xue J. et al. 2021. Dynamics of vegetation greenness and its response to climate change in Xinjiang over the past two decades. *Remote Sensing*, 13, 4063. DOI: 10.3390/rs13204063.
- Yonghua, Z. et al. 2022. Effects of human activity intensity on habitat quality based on nighttime light remote sensing: A case study of Northern Shaanxi, China. *Science of The Total Environment*, 851 (1), 158037.
- Yu, H., Bian, Z., Mu, S., Yuan, J., Chen, F. 2020. Effects of climate change on land cover change and vegetation dynamics in Xinjiang, China. *International Journal of Environmental Research and Public Health*, 17, 1–24.
- Zhang, J. et al. 2018. Effects of seasonal variability of climatic factors on vegetation coverage across drylands in northern China. *Land Degradation and Development*, 29 (6), 1782–1791.
- Zhang, Y., Gao, J., Liu, L., Wang, Z., Ding, M., Yang, X. 2013. NDVI-based vegetation changes and their responses to climate change from 1982 to 2011: A case study in the Koshi River Basin in the middle Himalayas. *Global and Planetary Change*, 108, 139–148.
- Zhao, H., Li, X., Ezizi, M., Yao, J. 2022. Changes in the characteristics of dry-wet periods in Xinjiang, China based on the SPEI index. *Atmosfera*, 35 (3), 483–496.
- Zhou, Q., Wei, X., Zhou, X., Cai, M., Xu, Y. 2019. Vegetation coverage change and its response to topography in a typical karst region: the Lianjiang River Basin in Southwest China. *Environmental Earth Sciences*, 78, 1–10.
- Zhuang, Q., Wu, S., Feng, X., Niu, Y. 2020. Analysis and prediction of vegetation dynamics under the background of climate change in Xinjiang, China. *PeerJ*, 8:e8282. DOI: 10.7717/peerj.8282.